Inorganic Chemistry
Article

Inorg. Chem. **2010**, *49*, 6035–6057 **6035**
DOI: 10.1021/ic100710d

Proton-Transfer Reactions to Half-Sandwich Ruthenium Trihydride Complexes Bearing Hemilabile P,N Ligands: Experimental and Density Functional Theory Studies†

Manuel Jiménez-Tenorio,* M. Carmen Puerta,* and Pedro Valerga

Departamento de Ciencia de Materiales e Ingeniería Metalúrgica y Química Inorgánica, Facultad de Ciencias, Universidad de Cádiz, 11510 Puerto Real, Cádiz, Spain

Salvador Moncho, Gregori Ujaque, and Agustí Lledós*

Departament de Química, Universitat Autònoma de Barcelona, 08193 Bellaterra, Barcelona, Spain

Received April 16, 2010

The trihydride complexes [Cp*RuH$_3$(κ^1-P-^{i}Pr$_2$PCH$_2$X)] [X = pyridine (Py), **2a**; quinoline (Quin), **2b**] have been prepared by reaction of the corresponding chloro derivatives [Cp*RuCl(κ^2-P,N-^{i}Pr$_2$PCH$_2$X)] [X = Py (**1a**), Quin (**1b**)] with NaBH$_4$ in methanol. Both **2a** and **2b** exhibit quantum-mechanical exchange coupling. The proton-transfer reactions to **2a** and **2b** using strong as well as weak proton donors have been experimentally and computationally studied. Density functional theory studies have been performed to analyze the stability of the proposed species, the hydrogen exchange, and the protonation pathway. The reactions with weak donors such as PhCOOH, indole, or salicylic acid in benzene or toluene result in the formation of hydrogen-bonded adducts between the proton donor and the pendant pyridine or quinoline group. However, in a more polar solvent such as dichloromethane, there is spectral evidence for the proton transfer to the hydride to yield a dihydrogen complex. The protonation with CF$_3$SO$_3$H in CD$_2$Cl$_2$ occurs in a stepwise manner. In a first step, the pendant pyridine or quinoline group is protonated to yield [Cp*RuH$_3$(κ^1-P-^{i}Pr$_2$PCH$_2$XH)]$^+$ [X = Py (**4a**) or Quin (**4b**)]. The NH proton is then transferred to the hydride and one molecule of dihydrogen is released, furnishing the cationic mono(dihydrogen) complexes [Cp*Ru(H$_2$)(κ^2-P,N-^{i}Pr$_2$PCH$_2$X)]$^+$ [X = Py (**5a**) or Quin (**5b**)]. These species are thermally stable and do not undergo irreversible rearrangement to their dihydride isomers. In the presence of an excess of acid, a second protonation occurs at the hydride site and the dicationic complexes [Cp*RuH$_4$(κ^1-P,N-^{i}Pr$_2$PCH$_2$XH)]$^{2+}$ [X = Py (**6a**) or Quin (**6b**)] are generated. These species are stable up to 273 K and consist of equilibrium mixtures between bis(dihydrogen) and dihydrido(dihydrogen) tautomeric forms. Above this temperature, **6a** and **6b** are converted into the corresponding cationic mono(dihydrogen) complexes **5a**/**5b**. The crystal structures of [Cp*RuCl(κ^2-P,N-^{i}Pr$_2$PCH$_2$Quin)] (**1b**), [Cp*RuH$_3$(κ^1-P-^{i}Pr$_2$PCH$_2$Quin)] (**2b**), [Cp*-RuH$_3$(κ^1-P-^{i}Pr$_2$PCH$_2$Py···H···OOCC$_6$H$_4$OH)] (**3a**), [Cp*Ru(H$_2$)(κ^2-P,N-^{i}Pr$_2$PCH$_2$Quin)][BAr′$_4$] (**5b**), [Cp*Ru-(N$_2$)(κ^2-P,N-^{i}Pr$_2$PCH$_2$Quin)][BAr′$_4$] (**8b**), and [Cp*Ru(O$_2$)(κ^2-P,N-^{i}Pr$_2$PCH$_2$Quin)][BAr′$_4$] (**9b**) are reported.

Introduction

Ruthenium trihydride complexes of the type [Cp*RuH$_3$-(L)] (L = PR$_3$,[1−5] AsPh$_3$,[6] SbPh$_3$,[6] N-heterocyclic carbene[7]) are an important class of polyhydrides. One of the main features of this class of compounds is their propensity to exhibit quantum-mechanical exchange coupling (QEC).[8,9] This behavior is related to high hydride mobility. In order for such a phenomenon to be observed, a low energy barrier

† Dedicated to Prof. Serafin Bernal in recognition of his contribution to inorganic chemistry, on the occasion of his retirement.

*To whom correspondence should be addressed. E-mail: manuel.tenorio@uca.es (M.J.-T.), carmen.puerta@uca.es (M.C.P.), agusti@klingon.uab.es (A.L.). Tel: +34 956 016340 (M.J.-T.). Fax: +34 956 016288 (M.J.-T.).

(1) Suzuki, H.; Lee, D. H.; Oshima, N.; Moro-oka, Y. *Organometallics* **1987**, *6*, 1569–1575.
(2) Arliguie, T.; Border, C.; Chaudret, B.; Devillers, J.; Poilblanc, R. *Organometallics* **1989**, *8*, 1308–1314.
(3) Arliguie, T.; Chaudret, B.; Jalon, F. A.; Otero, A.; Lopez, J. A.; Lahoz, F. J. *Organometallics* **1991**, *10*, 1888–1896.
(4) Johnson, T.; Coan, P. S.; Caulton, K. G. *Inorg. Chem.* **1993**, *32*, 4594–4599.
(5) Rodríguez, V.; Donnadieu, B.; Sabo-Etienne, S.; Chaudret, B. *Organometallics* **1998**, *17*, 3809–3814.
(6) Aneetha, H.; Jiménez-Tenorio, M.; Puerta, M. C.; Valerga, P. *J. Organomet. Chem.* **2002**, *663*, 151−157 and references cited therein.
(7) Jones, A. L.; McGrady, S.; Sirch, P.; Steed, J. W. *Chem. Commun.* **2005**, 5994–5996.
(8) Sabo-Etienne, S.; Chaudret, B. *Chem. Rev.* **1998**, *6*, 2077–2091.
(9) Maseras, F.; Lledós, A.; Clot, E.; Eisenstein, O. *Chem. Rev.* **2000**, *100*, 601–636.

Published on Web 06/04/2010

and a short path length are required for pairwise hydrogen exchange. This has prompted detailed spectroscopic and theoretical studies in order to account for the origin of the QEC phenomenon and also the dynamic behavior of the hydride ligands on these systems.[10−15] QEC has proven to be a hypersensitive indicator of weak interaction.[16] In this way, QEC can be modulated through hydrogen bonding. Thus, the addition of various proton donors such as methanol (MeOH), indole, phenol, or hexafluoroisopropanol to [Cp*-$RuH_3(PCy_3)$] leads to an increase of QEC between the hydride sites.[17,18] This has been interpreted in terms of a hydrogen-bonding interaction[19] between [Cp*$RuH_3(PCy_3)$] and the proton donors added. The protonation of [Cp*-$RuH_3(PR_3)$] (PR_3 = PPh_3, PCy_3) with a strong acid such as $HBF_4 \cdot OEt_2$ led to extensive dihydrogen evolution and dehydrogenation of one cyclohexyl ring of the PCy_3 ligand.[3] At variance with this, the trihydrides [Cp*$RuH_3(EPh_3)$] (E = As, Sb) were protonated by $HBF_4 \cdot OEt_2$ in CH_2Cl_2 at 193 K, furnishing the corresponding cationic bis(dihydrogen) complexes [Cp*Ru(η^2-H_2)$_2$(EPh_3)][BF_4], which were characterized in solution by T_1 and $^1J_{HD}$ measurements.[6] These species decompose at $T > 273$ K. [Cp*$RuH_4(PCy_3)$]$^+$ was identified as the species resulting from protonation of the hydrogen-bonded complex [Cp*$RuH_3(PCy_3)$]···[HOR] [R = CH-$(CF_3)_2$, $C(CF_3)_3$] by the corresponding ROH in a $CDClF_2$/$CDCF_3$ mixture at 200 K.[18] T_1 measurements for [Cp*RuH_4-(PCy_3)]$^+$ were consistent with a dihydrido(dihydrogen) structure [Cp*RuH_2(η^2-H_2)(PCy_3)]$^+$, although a bis(dihydrogen) structure [Cp*Ru(η^2-H_2)$_2$$(PCy_3)$]$^+$ was not ruled out.

We have now prepared Cp*Ru complexes bearing the hemilabile ligands diisopropylphosphinomethylpyridine (^{i}Pr_2PCH_2Py) and diisopropylphosphinomethylquinoline (^{i}Pr_2PCH_2Quin). The trihydride complexes [Cp*RuH_3(κ^1-P-^{i}Pr_2PCH_2X)] [X = pyridine (Py), quinoline (Quin)], with one dangling pyridine or quinoline group, have been synthesized and characterized. P,N-donor ligands such as pyridylphosphines PR_2Py and their relatives with CH_2 groups as spacers between the pyridine and the phosphorus atom have a great interest because of their potential hemilabile character because they can furnish complexes that behave as masked 16-electron coordinatively unsaturated species.[20,21] The presence of several competing protonation sites in [Cp*RuH_3-(κ^1-P-^{i}Pr_2PCH_2X)] leads to selectivity problems in the proton-transfer reaction, namely, protonation at the hydride site and protonation at the metal or nitrogen atom of the pendant pyridyl or quinolyl group.[22] On the other hand, the nitrogen atom in these groups may act as an internal base, which assists proton transfer to the hydride ligands. This fact has shown to be extremely important in reactions of hydride complexes bearing PPh_2Py. Thus, the use of the phosphine PPh_2Py instead of PPh_3 in complexes of the type [Cp*-$RuH(P)_2$] enormously alters the kinetic control of the proton-transfer reactions over this compound and its chemical behavior.[23] Thus, the reaction at low temperature of [Cp*-$RuH(PPh_2Py)_2$] with 1 equiv of HBF_4 yields the dihydride [Cp*$RuH_2(PPh_2Py)_2$][BF_4], whereas a second protonation leads to the dihydrogen-bonded complex [Cp*RuH{H···$HPyPPh_2$}(PPh_2Py)][BF_4]$_2$.

In this work, we describe the synthesis and characterization of Cp*Ru trihydride and related complexes containing the hemilabile ligands ^{i}Pr_2PCH_2Py or ^{i}Pr_2PCH_2Quin and the study by variable-temperature (VT) NMR spectroscopy of their proton-transfer reactions with both weak and strong proton donors. Density functional theory (DFT) studies have been performed to analyze the stability of the proposed species, the hydrogen exchange, and the protonation pathway. These studies suggest that the protonation reaction occurs in two steps. First, the pendant nitrogen atom is protonated and a dihydrogen-bonded hydride is formed. Then, the NH proton is transferred to the hydride, releasing one molecule of dihydrogen and furnishing the dihydrogen complex [Cp*-Ru(H_2)(κ^2-P,N-Me_2PCH_2Py)]$^+$, which is more stable than its ruthenium(IV) dihydride isomer. In the presence of an excess of acid, a second protonation occurs, leading to the bis(dihydrogen) complex [Cp*Ru(η^2-H_2)$_2$(κ^1-P-Me_2PCH_2PyH)]$^{2+}$ as the most stable species. These results are fully consistent with the experimental observations hereby presented.

Results and Discussion

1. Preparation and Characterization of Halo- and Trihydrido Complexes. The tetramer [{Cp*RuCl}$_4$] reacts cleanly with either ^{i}Pr_2PCH_2Py or ^{i}Pr_2PCH_2Quin in petroleum ether, furnishing the corresponding chloro complex [Cp*RuCl(κ^2-P,N-^{i}Pr_2PCH_2Py)] (**1a**) or [Cp*RuCl(κ^2-P,N-^{i}Pr_2PCH_2Quin)] (**1b**) in good yield. **1a** is a red-orange compound that exhibits NMR features consistent with a three-legged-piano-stool structure, involving a κ^2-P,N chelating phosphinomethylpyridine. In such a geometry, the protons of the methylene group linking the phosphorus atoms and the pyridine are inequivalent and appear as a characteristic ABX pattern in the ^{1}H NMR spectrum. In contrast with this, **1b** is almost black with a greenish hue. Its ^{1}H NMR spectrum in C_6D_6 shows broad resonances that get sharper as the temperature increases, indicative of the occurrence of a dynamic process in solution. Thus, the CH_2 protons at 25 °C appear as two broad signals, consistent with an unresolved ABX spin system. At 70 °C, the two broad signals have coalesced to one broad doublet, which suggests the equivalence in the NMR time scale of these two protons. This can be

(10) Heinekey, D. M.; Payne, N. G.; Sofield, C. D. *Organometallics* **1990**, *9*, 2643–2645.
(11) Limbach, H.-H.; Scherer, G.; Maurer, M.; Chaudret, B. *Angew. Chem., Int. Ed. Engl.* **1992**, *31*, 1369–1372.
(12) (a) Jarid, A.; Moreno, M.; Lledós, A.; Lluch, J. M.; Bertrán, J. *J. Am. Chem. Soc.* **1993**, *115*, 5861–5862. (b) Jarid, A.; Moreno, M.; Lledós, A.; Lluch, J. M.; Bertrán, J. *J. Am. Chem. Soc.* **1995**, *117*, 1069–1075.
(13) Clot, E.; Le Forestier, C.; Eisenstein, O.; Pelissier, M. *J. Am. Chem. Soc.* **1995**, *117*, 1797–1799.
(14) Limbach, H.-H.; Ulrich, S.; Gründemann, S.; Buntkowsky, G.; Sabo-Etienne, S.; Chaudret, B.; Kubas, G. J.; Eckert, J. *J. Am. Chem. Soc.* **1998**, *120*, 7929–7943.
(15) Guari, Y.; Ayllon, J. A.; Sabo-Etienne, S.; Chaudret, B.; Hessen, B. *Inorg. Chem.* **1998**, *37*, 640–644.
(16) Kuhlman, R.; Clot, E.; Leforestier, C.; Streib, W. E.; Eisenstein, O.; Caulton, K. G. *J. Am. Chem. Soc.* **1997**, *119*, 10153–10169.
(17) Ayllon, J. A.; Sabo-Ettiene, S.; Chaudret, B.; Ulrich, S.; Limbach, H.-H. *Inorg. Chim. Acta* **1997**, *259*, 1–4.
(18) Gründemann, S.; Ulrich, S.; Limbach, H.-H.; Golubev, N. S.; Denisov, G. S.; Epstein, L. M.; Sabo-Etienne, S.; Chaudret, B. *Inorg. Chem.* **1999**, *38*, 2550–2551.
(19) Epstein, L. M.; Shubina, E. S. *Coord. Chem. Rev.* **2002**, *231*, 165–181.
(20) Grotjahn, D. B. *Dalton Trans.* **2008**, 6497–6508.
(21) Espinet, P.; Soulantica, K. *Coord. Chem. Rev.* **1999**, *193−195*, 499–556.
(22) Besora, M.; Lledós, A.; Maseras, F. *Chem. Soc. Rev.* **2009**, *38*, 957–966.
(23) Jalón, F. A.; Manzano, B. R.; Caballero, A.; Carrión, M. C.; Santos, L.; Espino, G.; Moreno, M. *J. Am. Chem. Soc.* **2005**, *127*, 15364–15365.

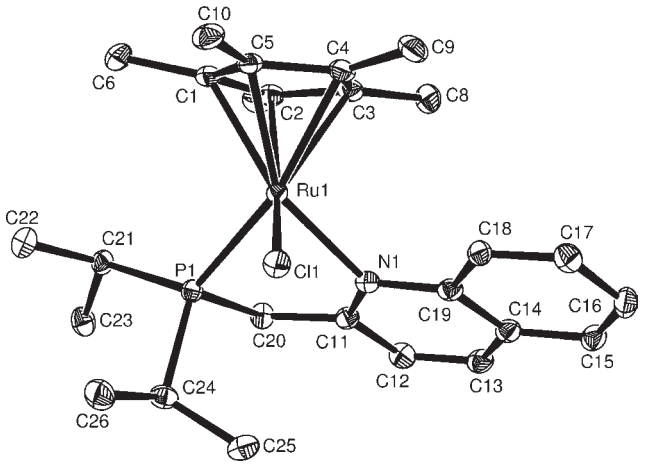

Figure 1. ORTEP drawing (50% thermal ellipsoids) of **1b**. Hydrogen atoms have been omitted. Selected bond lengths (Å) and angles (deg) with estimated standard deviations in parentheses: Ru1−P1 2.3135(7), Ru1−N1 2.1712(19), Ru1−Cl1 2.4867(9), Ru1−C1 2.192(2), Ru1−C2 2.164(2), Ru1−C3 2.192(2), Ru1−C4 2.211(2), Ru1−C5 2.181(2); P1−Ru1−N1 79.23(5), P1−Ru1−Cl1 95.42(2), N1−Ru1−Cl1 91.98(6).

Scheme 1

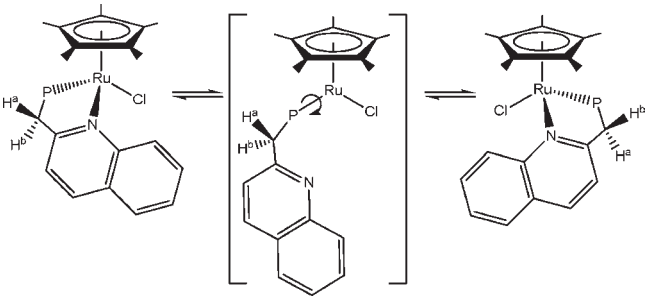

explained in terms of dissociation of the quinoline group from the ruthenium atom and recoordination on the other side of the molecule upon rotation around the Ru−P bond. This can be viewed as an effective racemization, which involves the mutual exchange of the two CH_2 protons through the intermediacy of a 16-electron intermediate containing one κ^1-P-phosphinomethylquinoline ligand, as shown in Scheme 1.

Complexes of the type Cp*RuCl(P) are well-known. They are usually blue or purple in color and in our system constitute an obvious choice as intermediate species. Interestingly, when recorded in CD_2Cl_2 as the solvent, very well-resolved NMR spectra were obtained for **1b**, in contrast with the behavior observed in a nonpolar solvent such as C_6D_6. The observed differences in color between compounds **1a** and **1b**, as well as the dynamic behavior of **1b** in solution, prompted us to examine the solid-state structure of **1b** by X-ray analysis. An ORTEP view of complex **1b** is shown in Figure 1, together with the most relevant bond distances and angles.

Crystal structure analysis of the complex showed that **1b** adopts standard three-legged-piano-stool geometry in the solid state. The quinoline rings are planar, but the five-membered ring formed by Ru1, P1, C20, C11, and N1 is not planar. The plane defined by the quinoline forms an angle of 37.8° with the plane defined by Ru1, P1, and C20. All of the Ru−P, Ru−N, and Ru−Cl separations, as well as the Ru−C bond distances, are

Scheme 2

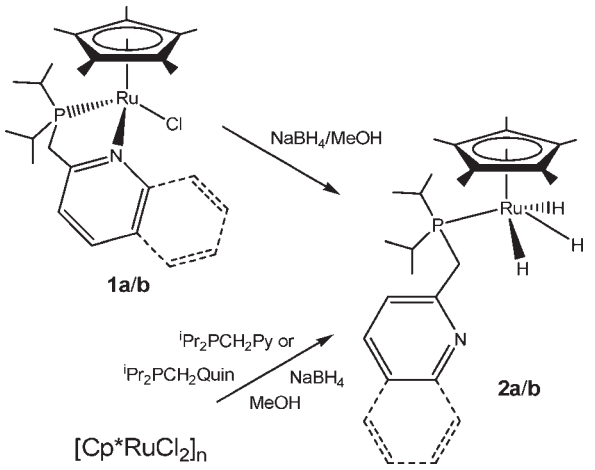

comparable with values previously reported in the literature for related complexes, i.e., in [Cp*RuCl(dippe)],[24] or in [{η^5-$C_5H_4C(CH_3)_2CH(PPh_2)C_5H_4N$}Ru($PPh_3$)][$PF_6$].[25]

1a and **1b** react with an excess of $NaBH_4$ in MeOH to give the trihydride complexes [Cp*RuH_3(κ^1-P-^{i}Pr_2PCH_2-Py)] (**2a**) or [Cp*RuH_3(κ^1-P-^{i}Pr_2PCH_2Quin)] (**2b**). The reactions can be carried out at room temperature, but because of the strong evolution of dihydrogen and the observed exothermic effects, it is more convenient and safe to perform the syntheses at 0 °C by using an ice bath. Complexes **2a** and **2b** can also be prepared directly from $[Cp^*RuCl_2]_n$ by reaction with either ^{i}Pr_2PCH_2Py or ^{i}Pr_2PCH_2Quin and an excess of $NaBH_4$ in MeOH, presumably through the intermediacy of the corresponding ruthenium(III) derivative of the type [Cp*$RuCl_2$(^{i}Pr_2-PCH_2X)] (X = Py, Quin), which was not isolated (Scheme 2).

Both **2a** and **2b** are crystalline materials, very soluble in both polar and nonpolar solvents, that exhibit medium-strong ν(Ru−H) bands in their IR spectra near 1989 cm^{-1}. The crystal structure of **2b** was determined by means of X-ray analysis. An ORTEP view of the complex **2b** is shown in Figure 2, together with the most relevant bond distances and angles.

The structure of **2b** consists of a packing of discrete molecules of the trihydride complex. The nitrogen atom of the quinoline group points away from the hydrides and does not show any interaction either intra- or intermolecular with these ligands. The geometry around the ruthenium atom in **2b** can be described as a four-legged piano stool, an arrangement very similar to that observed in the structures of [Cp*RuH_3(PPh_3)],[1] [Cp*RuH_3(P(pyrrolyl)$_3$)],[26] and [CpRuH_3(PPh_2^{i}Pr)].[27] The hydride ligands H1 and H3 adopt a mutually transoid disposition, whereas the hydride H2 is transoid to the phosphorus atom. The ruthenium−hydride separations between 1.51 and 1.54 Å compare well with the Ru−H bond distances in the

(24) de los Ríos, I.; Jiménez-Tenorio, M.; Padilla, J.; Puerta, M. C.; Valerga, P. *J. Chem. Soc., Dalton Trans.* **1996**, 377–381.
(25) Brunner, H.; Valeris, C.; Zabel, M. *New J. Chem.* **2000**, *24*, 275–279.
(26) Gründemann, S.; Limbach, H.-H.; Rodríguez, V.; Donnadieu, B.; Sabo-Etienne, S.; Chaudret, B. *Ber. Bunsenges. Phys. Chem.* **1998**, *102*, 344–353.
(27) Osipov, A. L.; Gutsulyak, D. V.; Kuzmina, L. G.; Howard, J. A. K.; Lemenovskii, D. A.; Süss-Fink, G.; Nikonov, G. I. *J. Organomet. Chem.* **2007**, *692*, 5081–5085.

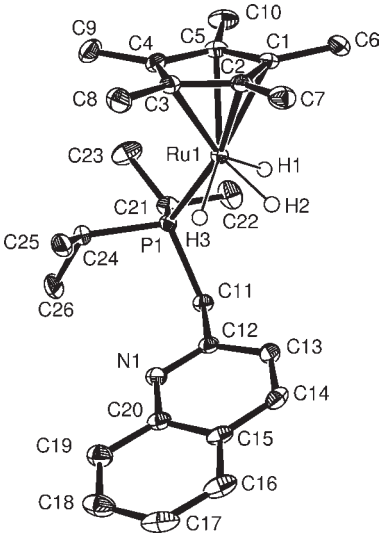

Figure 2. ORTEP drawing (50% thermal ellipsoids) of **2b**. Hydrogen atoms except hydride have been omitted. Selected bond lengths (Å) and angles (deg) with estimated standard deviations in parentheses: Ru1−P1 2.2574(9), Ru1−H1 1.51(2), Ru1−H2 1.51(2), Ru1−H3 1.54(2), Ru1−C1 2.2130(18), Ru1−C2 2.2291(18), Ru1−C3 2.2868(18), Ru1−C4 2.3133(17), Ru1−C5 2.2554(17), H1···H2 1.70, H2···H3 1.55; P1−Ru1−H2 94.9(8), P1−Ru1−H1 74.4(8), P1−Ru1−H3 70.5(7), H1−Ru1−H2 68.5(10), H1−Ru1−H3 113.7(11), H2−Ru1−H3 60.9(10).

other discrete $[(C_5R_5)RuH_3P]$ (R = H, Me) complexes that have been structurally characterized (within the uncertainty affecting the position of the hydride ligands determined by X-ray crystallography).[1,26,27] The values determined for the Ru−H bond distances and their arrangement around ruthenium lead to rather short hydride−hydride separations, in the interval of 1.55−1.70 Å.

2. Hydrogen Exchange in the Trihydrides. At room temperature, the three hydrides in **2a**/**2b** are equivalent and appear as one doublet in the high-field region of the ^{1}H NMR spectra. These hydride resonances exhibit minimum longitudinal relaxation times $(T_1)_{min}$ of 189 ms for **2a** and 184 ms for **2b** (400 MHz, CD_2Cl_2). These values are consistent with the relatively short hydride−hydride separations found by X-ray crystallography. In contrast with **1a**/**1b**, the CH_2 protons of the phosphinomethylpyridine or phosphinomethylquinoline ligands are equivalent in the ^{1}H NMR spectra of **2a**/**2b**, giving rise to one doublet. This is characteristic of the κ^1-P-coordination mode for these ligands. As occurs in other Cp*RuH_3(P) [P = P^{i}Pr$_3$, PCy_3, P(pyrrolyl)$_3$] complexes, QEC has also been observed for the hydride ligands in **2a** and **2b**. At low temperature, the hydrides become inequivalent, giving rise to a complex multiplet in the ^{1}H NMR spectra. The VT ^{1}H NMR spectra of **2a**/**2b** in the high-field region (CD_2Cl_2) are shown in Figure 3.

The VT ^{1}H NMR spectra were successfully simulated assuming an ABCX spin system, where A−C are the hydrides and X represents the phosphorus atom. At 193 K, the QEC constants $J(H_A,H_B) = J(H_A,H_C) = {}^{QEC}J_{HH}$ derived by NMR line-shape analyses have values of 176 Hz for **2a** and of 185 Hz for **2b**. The values for these constants are temperature-dependent, as is characteristic in QEC, and at 213 K, their values increase to 273 and 311 Hz, respectively. The dynamic process of two-site exchange between the central (H_A) and side hydride ligands (H_B and H_C) has an energy barrier $\Delta G^{\ddagger}$ of 41.7 ± 0.8 kJ mol^{-1} for **2a** and 42.4 ± 0.7 kJ mol^{-1} for **2b** (determined by VT-NMR line-shape analysis). These values are intermediate between 40 kJ mol^{-1} reported for the hydride-exchange energy barrier in $[CpRuH_3(PPh_3)]$[10] and 46 kJ mol^{-1} in the case of $[Cp^*RuH_3(PCy_3)]$.[2,8] The QEC constants in our systems also have values that are intermediate between those reported for $[Cp^*RuH_3(PPh_3)]$ (290 Hz at 190 K) and $[Cp^*RuH_3(PCy_3)]$ (60 Hz at 190 K).[8] This can be interpreted in terms of control of the exchange coupling and the hydride-exchange barrier as a function of the basicity of the ancillary ligands, placing ^{i}Pr$_2$PCH$_2$X (X = Py, Quin) between PPh_3 and PCy_3 on this scale.

We have theoretically studied the hydrogen-exchange process in the model complex $[Cp^*RuH_3(\kappa^1$-P-Me$_2$-PCH$_2$Py)] (**2a$_m$**). The optimized geometries of the minimum and the transition state for the hydrogen exchange are depicted in Figure 4.

Two different conformations, both with a trihydride nature but differing in the orientation of the pyridine ring, were obtained as minima for the initial complex **2a$_m$**. The structure with the nitrogen atom of the pyridine pointing away from the hydrides is 8.0 kJ mol^{-1} more stable than the conformer with the nitrogen atom pointing toward the hydrides. Indeed, this is the conformation found in the X-ray structure of **2b** (Figure 2). The transition state for the exchange between central and lateral hydrides shows a η^2-H_2 complex-like nature, as can be inferred from the H−H distance and the H−Ru−H angle between the exchanging atoms (0.872 Å and 30.0°, respectively). As found in previous theoretical studies of hydrogen exchange in trihydrides, this process entails approaching and rotating the two exchanging hydrogen atoms.[12,13,28] The calculated Gibbs energy of activation is 63 kJ mol^{-1}, slightly higher than the values determined for **2a** and **2b** by VT-NMR line-shape analysis but in the range of the theoretically calculated barriers for systems exhibiting QEC.[12,13,28] Calculations confirm that in these ruthenium trihydrides exists a pathway with a low barrier and a short path length for the hydrogen exchange, as required for observation of QEC.

3. Reactions with Weak Proton Donors: Hydrogen and Dihydrogen Bonding. The reactions of **2a**/**2b** with PhCOOH or indole in the ratio 1:1 complex/proton donor in CD_2Cl_2 were monitored in the temperature range −80 to +25 °C. Very slight changes in the chemical shifts were observed in the ^{1}H and ^{31}P{^{1}H} NMR spectra compared to the values for **2a**/**2b** in the absence of the proton donor. The protic hydrogen of the donor appears in the ^{1}H NMR spectra in all cases as a broad or very broad low-field signal, at a chemical shift that varies considerably with the temperature. QEC and rapid hydride exchange are maintained. As a general tendency, the values of the QEC constants show a slight to moderate increase. The largest increase has been observed in the case of **2a** upon the addition of indole, in which ${}^{QEC}J_{HH}$ changes from 176 to 236 Hz (Table 1).

(28) Castillo, A.; Barea, G.; Esteruelas, M. A.; Lahoz, F. J.; Lledós, A.; Maseras, F.; Modrego, J.; Oñate, E.; Oro, L. A.; Ruiz, N.; Sola, E. *Inorg. Chem.* **1999**, *38*, 1814–1824.

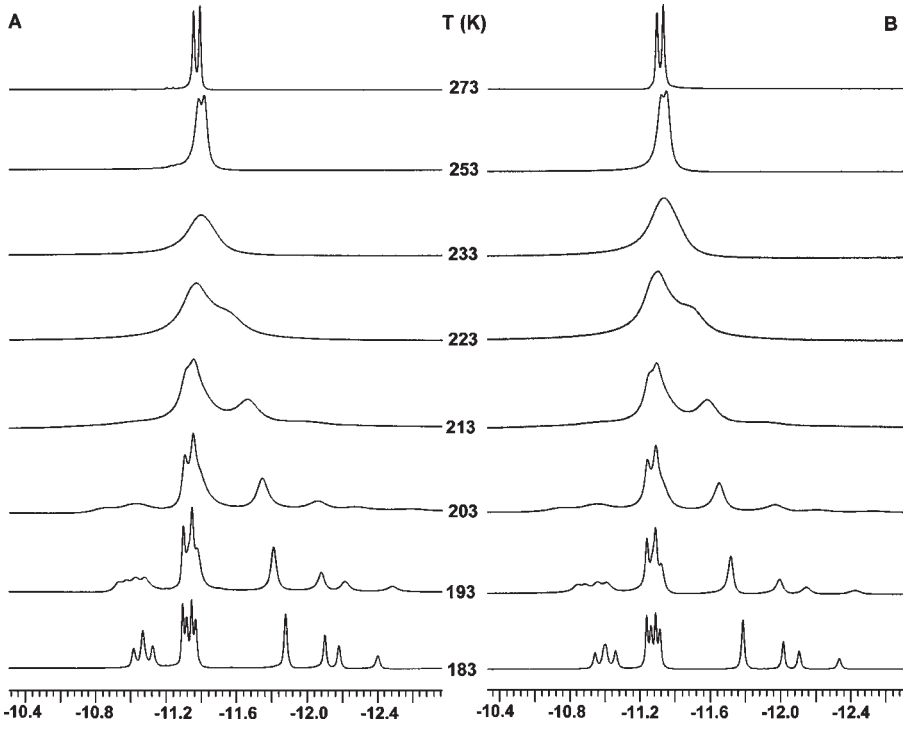

Figure 3. VT ^{1}H NMR spectra (hydride region, 600 MHz, CD_2Cl_2) of **2a** (A) and **2b** (B).

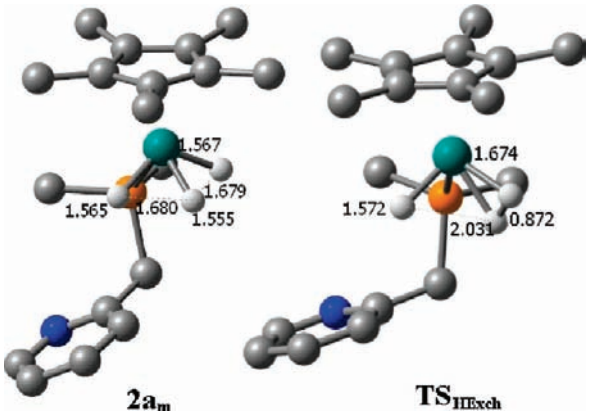

Figure 4. Optimized geometries of the trihydride minimum and the transition state for the hydrogen exchange in $\mathbf{2a_m}$. Hydrogen atoms except hydrides have been omitted.

In contrast with this, it has been reported that the addition of various proton donors to $[Cp^*RuH_3(PCy_3)]$ leads to a significant increase of QEC between the hydride sites, indicative of the formation of dihydrogen bonds between the hydride ligands and the proton donor.[17,18] In our case, the values of $(T_1)_{min}$ for the hydride resonances in the presence of the proton donor do not vary to a great extent compared to the values measured in the absence of PhCOOH or indole. However, the H···H separations expected in a dihydrogen bond should be in the range 1.61−2.10 Å.[19,20] This distance would be on the same order as the hydride−hydride separations already present in **2a**/**2b**. Therefore, a significant shortening in $(T_1)_{min}$ is not expected even in the case of the formation of dihydrogen bonds. These data suggest that the interaction between the hydride ligands in **2a**/**2b** and the proton of either PhCOOH or indole is not very significant. We have interpreted our data in terms of the occurrence of an equilibrium involving the formation of dihydrogen-bonded species $[Cp^*RuH_2(H\cdots HA)(\kappa^1\text{-P-}^iPr_2PCH_2X)]$ (HA = PhCOOH, indole; X = Py, Quin) as well as species containing one standard hydrogen bond between the proton donor and the nitrogen atom of the pendant pyridyl or quinolyl group in which the hydride ligands do not participate in this interaction (Chart 1). Our data suggest that the equilibrium is shifted toward the species having hydrogen bonding with the nitrogen atom.

We have studied as well the interaction of **2a**/**2b** with salicylic acid (Table 1). The molecule of salicylic acid has two protons of different acidity arranged in such a way that the simultaneous interaction with both the nitrogen atom of the pendant group and the hydride ligands might be feasible. Upon the addition of 1 equiv of salicylic acid to **2b** in dichloromethane (DCM), $^{QEC}J_{HH}$ increased slightly to a value of 202 Hz. $(T_1)_{min}$ of the hydride resonance changed also very slightly to a value of 200 ms. However, the appearance of the VT ^{1}H NMR spectra profile was different from that obtained for the cases in which PhCOOH or indole were added (Figure 5).

With salicylic acid, as the temperature increases, the second-order multiplet for the hydrides becomes a broad resonance that does not resolve into one doublet, resulting from rapid intramolecular hydride exchange. Furthermore, at 298 K, the spectrum becomes featureless in the hydride region (Figure 5B). The $^{31}P\{^1H\}$ NMR at 193 K shows one broad signal centered at 96.6 ppm, which is significantly shifted from the position of the resonance for **2b** at the same temperature (88.4 ppm). As the temperature increases, the phosphorus resonance becomes sharper. An almost identical behavior was observed in the case of compound **2a** in the presence of 1 equiv of salicylic acid (Figure 5A). However, at variance with **2b**, $(T_1)_{min}$ for the hydride resonance decreases to a value of 16 ms at 273 K. This value is very short and consistent with the formation

Table 1. Values of $^{QEC}J_{HH}$ and $(T_1)_{min}$ for the Hydride Resonances and of δ for the Most Relevant ^1H and $^{31}P\{^1H\}$ NMR Resonances of **2a**/**2b** in the Presence of Weak Proton Donors (400 MHz, CD_2Cl_2)

entry	complex	proton donor	$^{QEC}J_{HH}$ (Hz)[a]	$(T_1)_{min}$ (ms)	^1H δ (ppm):[b] RuH_3, $C_5(CH_3)_5$	$^{31}P\{^1H\}$ δ (ppm)[b]
1	**2a**		176	189	−11.39, 1.92	86.8
2	**2a**	PhCOOH	184	175	−11.36, 1.95	89.6
3	**2a**	indole	236	192	−11.18, 2.00	87.4
4	**2a**	salicylic acid	225	16.7	−11.32, 1.93	94.3
5	**2b**		185	184	−11.33, 1.93	88.4
6	**2b**	PhCOOH	185	189	−11.30, 1.92	89.8
7	**2b**	indole	195	186	−11.31, 1.93	87.5
8	**2b**	salicylic acid	202	200	−11.26, 1.92	96.6

[a] At 193 K. [b] At 203 K.

Chart 1

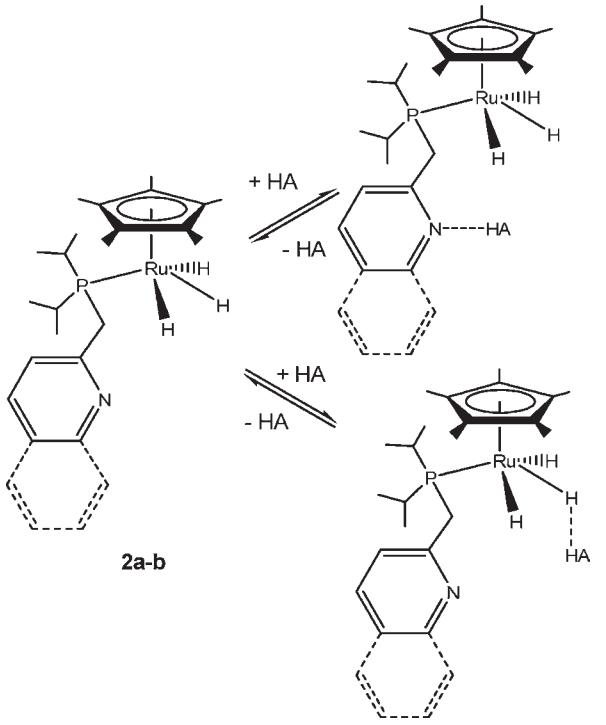

of species containing at least one dihydrogen ligand. We have rationalized this behavior by considering the enhanced acidity of salicylic acid compared to other weak proton donors due to the presence of a hydrogen-bond donor near the carboxyl group. Thus, in a polar solvent such as CD_2Cl_2, salicylic acid transfers one proton to the nitrogen atom of the pendant groups in either **2a** or **2b**, furnishing tightly hydrogen-bonded ion pairs (Chart 2).

In the case of **2a**, a further equilibrium takes place in which the proton on the nitrogen atom is transferred to the hydrides, leading to a cationic dihydrogen complex that may, in fact, contain up to two dihydrogen ligands, given the short $(T_1)_{min}$ value of 16.7 ms measured for this system (Chart 3).

We carried out an attempt to isolate the product resulting from the reaction of **2a** with salicylic acid. Thus, an orange crystalline material was obtained upon treatment of a toluene solution of **2a** with 1 equiv of salicylic acid at room temperature. At variance with **2a**, this product was not soluble in petroleum ether. Its IR spectrum showed a ν(Ru−H) band at 1979 cm^{-1} and one band attributable to ν(C=O) at 1596 cm^{-1}. Recrystallization from toluene/petroleum ether afforded crystals suitable for X-ray structure analysis, which showed this compound to be the hydrogen-bonded supramolecular aggregate [Cp*RuH_3(κ^1-P-^{i}Pr$_2$PCH_2Py···H···OOC$_6H_4$OH)] (**3a**). An ORTEP view of this compound is shown in Figure 6, together with the most relevant bond distances and angles.

The structure of compound **3a** consists of molecules of the trihydride complex **2a** and of salicylic acid assembled through a strong hydrogen bond between the hydrogen atom of the carboxylic group and the nitrogen atom of the pyridine substituent. The geometry and the dimensions of the trihydride complex moiety do not differ much from those found for **2b** by X-ray crystallography. The nitrogen atom N1 of the pyridine and the oxygen atom O1 of the salicylic acid are linked by a strong hydrogen bond involving the atom H1b. This hydrogen atom is essentially equidistant from O1 [1.25(3) Å] and N1 [1.29(3) Å]. The angle O1−H1b···N1 of 176(2)° indicates that these three atoms are colinear. There is another hydrogen bond within the salicylic acid moiety involving the hydrogen atom H3b and the oxygen atoms O1 and O2. However, in this case, the hydrogen bond is unsymmetrical and the H3b···O2 separation is much longer [1.81(3) Å]. There are no intra- or intermolecular interactions with hydride ligands. The Ru−H separations range from 1.48(2) to 1.55(2) Å, being unexceptional. The supramolecular arrangement of the trihydride complex and salicylic acid strongly linked by a symmetrical hydrogen bond is similar to that found by X-ray crystallography in the structure of the adduct bis[1,2-bis(4′-pyridyl)ethene] (2*R*,3*R*)-tartaric acid (2*R*,3*R*)-tartrate.[29]

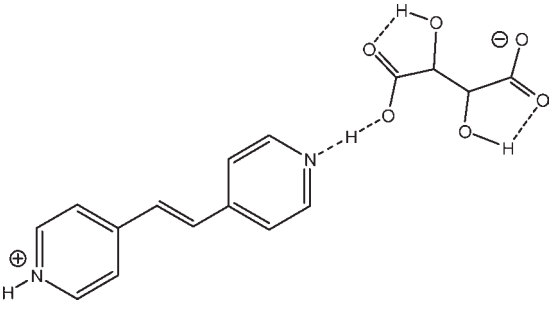

In this compound, a partial transfer of hydrogen occurs, manifested in the almost centered O···H···N interaction (bond distances: O···H 1.277 Å; N···H

(29) Farrell, D. M. M.; Ferguson, G.; Lough, A. J.; Glidewell, C. *Acta Crystallogr., Sect. B: Struct. Sci.* **2002**, *58*, 272–288.

1.278 Å). Likewise, in the case of **3a**, a partial transfer of the hydrogen atom from the salicylic acid to the nitrogen atom of the pyridine has also occurred, furnishing an aggregate that can be viewed as an intermediate situation between an adduct of **2a** with salicylic acid and an ion pair of the cation $[Cp^*RuH_3(\kappa^1\text{-P-}^i Pr_2PCH_2PyH)]^+$ with one salicylate anion.

Recent work has pointed out the profound effect that the nature of the solvent can have on the outcome of the protonation of neutral hydrides.[30] Thus, the polarity of the solvent plays a crucial role in determining the position of the equilibrium in the proton-transfer reactions shown in Charts 2 and 3. The NMR spectra of **3a** in C_6D_6 or toluene-d_8 differ considerably from those recorded in CD_2Cl_2. At 298 K, one doublet is observed in the hydride region of the ^{1}H NMR spectrum, whereas in CD_2Cl_2 at the same temperature, the spectrum shows an extremely broad resonance that almost merges with the baseline (Figure 5A). T_1 values measured at 298 K for the hydride signal in CD_2Cl_2 and in C_6D_6 are 21 and 550 ms, respectively. This observation is fully consistent with the fact that equilibrium shifts in favor of ionic structures because of the cooperative effect of hydrogen bonding with polar neighbors as the solvent polarity increases.[31] This has a remarkable effect on determining the position of the proton-transfer equilibrium involving transition-metal hydrides, as has recently been demonstrated in the case of $[RuH_2\{P(CH_2CH_2PPh_2)_3\}]$.[32]

4. Computational Study of Hydrogen Bonding with Weak Acids. The formation of hydrogen-bonded adducts was investigated with indole, using the model system $\mathbf{2a_m}$. From previous computational studies on hydrogen-bonded adducts between transition-metal trihydrides and weak proton donors, it arises that $\mathbf{2a_m}$ has five potential hydrogen-bonding sites: the nitrogen atom of the ligand, the three hydrides, and the metal.[33,34] To account for all of the possible hydrogen-bonded minima, we optimized the adduct between indole and $\mathbf{2a_m}$, starting from different regions around the metal and pyridine. In this way, three stable hydrogen-bonded structures were obtained, as shown in Figure 7 (top).

In the adduct $\mathbf{2a_m \cdot indole^{NH}}$, a normal hydrogen bond occurs between the nitrogen of the pyridyl group and the indole. The other two structures ($\mathbf{2a_m \cdot indole^{H1}}$ and $\mathbf{2a_m \cdot indole^{H2}}$) both exhibit a bifurcated dihydrogen bond between the proton donor and two hydride ligands: the central hydrogen atom and that on the side of the pyridyl nitrogen atom ($\mathbf{2a_m \cdot indole^{H1}}$) and the central atom and that away from the pyridyl nitrogen atom ($\mathbf{2a_m \cdot indole^{H2}}$). Recent studies have pointed out that in M−H···HA dihydrogen-bonded structures the proton could be interacting with both the metal atom and the hydride ligand.[34] The relatively short Ru···H(O) distances (2.841 Å in $\mathbf{2a_m \cdot indole^{H1}}$ and 2.792 Å in $\mathbf{2a_m \cdot indole^{H2}}$) and the almost linear Ru···H−O angles (169.5° in $\mathbf{2a_m \cdot indole^{H1}}$ and 174.0° in $\mathbf{2a_m \cdot indole^{H2}}$) suggest significant participation of the metal atom to hydrogen bonding.[34] The most stable adduct in DCM is $\mathbf{2a_m \cdot indole^{H1}}$ ($\Delta E_{DCM} = -28.8$ kJ

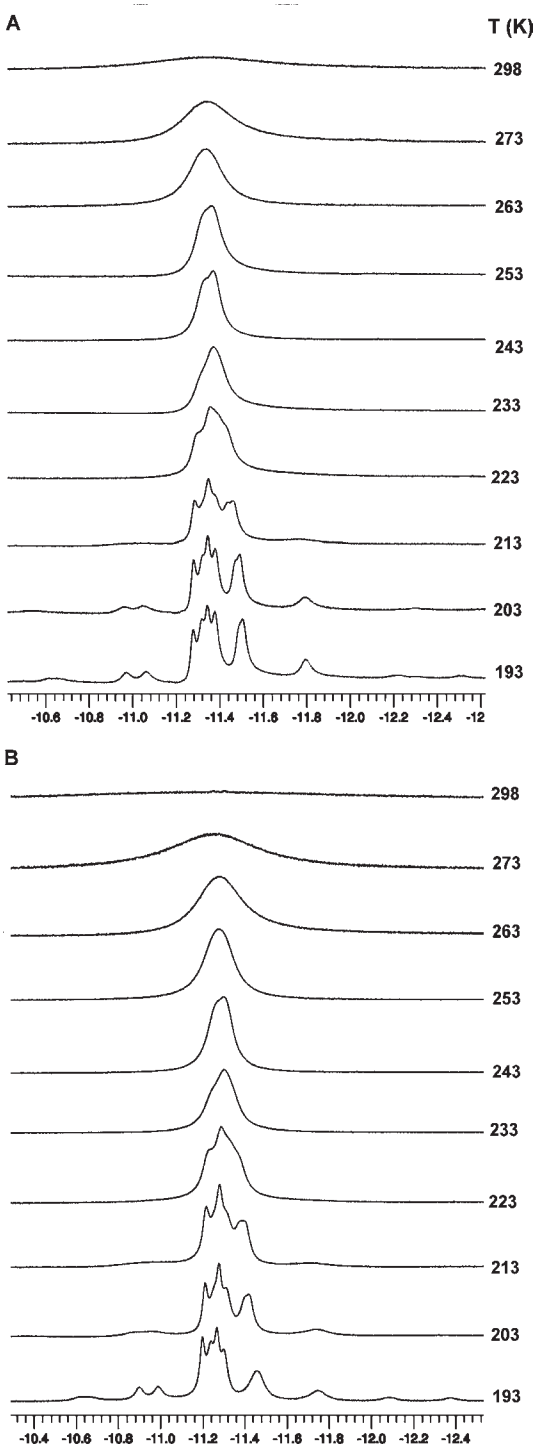

Figure 5. VT ^{1}H NMR spectra (hydride region, 400 MHz, CD_2Cl_2) of samples made by the addition of 1 equiv of salicylic acid to **2a** (A) or **2b** (B).

(30) (a) Dub, P. A.; Baya, M.; Houghton, J.; Belkova, N. V.; Daran, J.-C.; Poli, R.; Epstein, L. M.; Shubina, E. S. *Eur. J. Inorg.* **2007**, 2813–2826. (b) Dub, P. A.; Belkova, N. V.; Filippov, O. A.; Daran, J.-C.; Epstein, L. M.; Lledós, A.; Shubina, E. S.; Poli, R. *Chem.—Eur. J.* **2010**, *16*, 189–201.

(31) Sharif, S.; Denisov, G. S.; Toney, M. D.; Limbach, H.-H. *J. Am. Chem. Soc.* **2006**, *128*, 3375–3387.

(32) Belkova, N. V.; Gribanova, T. N.; Gutsul, E. I.; Minyaev, R. M.; Bianchini, C.; Peruzzini, M.; Zanobini, F.; Shubina, E. S.; Epstein, L. M. *J. Mol. Struct.* **2007**, *844−845*, 115–131.

(33) Bakhmutova, E. V.; Bakhmutov, V. I.; Belkova, N. V.; Besora, M.; Epstein, L. M.; Lledós, A.; Nikonov, G. I.; Shubina, E. S.; Tomàs, J.; Vorontsov, E. V. *Chem.—Eur. J.* **2004**, *10*, 661–671.

(34) (a) Belkova, N. V.; Revin, P. O.; Besora, M.; Baya, M.; Epstein, L. M.; Lledós, A.; Poli, R.; Shubina, E. S.; Vorontsov, E. V. *Eur. J. Inorg.* **2006**, 2192–2209. (b) Belkova, N. V.; Besora, M.; Baya, M.; Dub, P. A.; Epstein, L. M.; Lledós, A.; Poli, R.; Revin, P. O.; Shubina, E. S. *Chem.—Eur. J.* **2008**, *14*, 9921–9934.

Chart 2

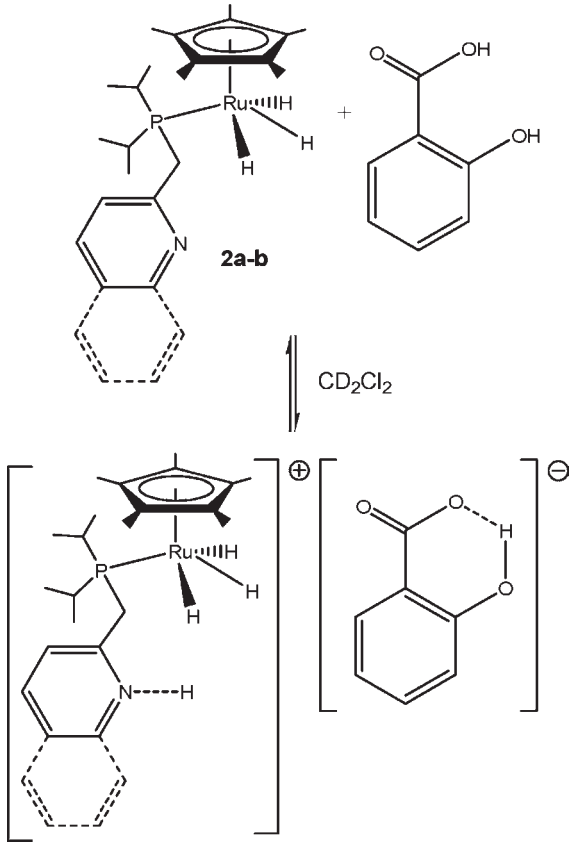

Chart 3

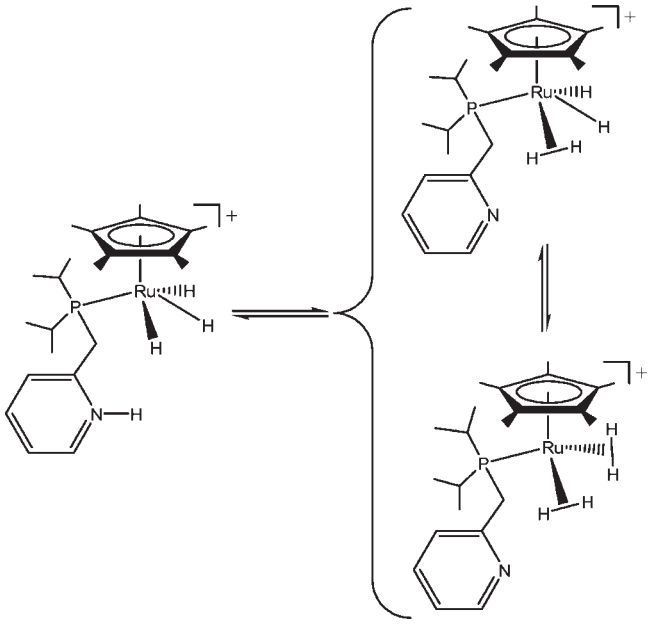

mol^{-1} relative to separated species), involving the bifurcated interaction with the lateral hydride on the nitrogen-atom side and the central hydride. The other dihydrogen-bonded structure ($\mathbf{2a_m \cdot indole^{H2}}$) is the less stable minimum ($\Delta E_{DCM} = -15.1$ kJ mol^{-1}). The species $\mathbf{2a_m \cdot indole^{NH}}$ containing a standard hydrogen bond between the proton donor and the nitrogen atom of the pendant pyridyl group is only marginally less stable ($\Delta E_{DCM} = -19.7$ kJ

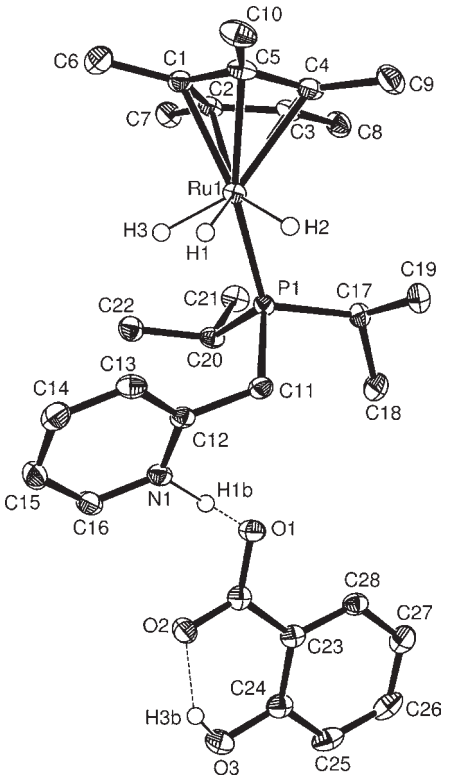

Figure 6. ORTEP drawing (50% thermal ellipsoids) of **3a**. Hydrogen atoms except hydride, H1b, and H3b have been omitted. Selected bond lengths (Å) and angles (deg) with estimated standard deviations in parentheses: Ru1−P1 2.2519(7), Ru1−H1 1.55(2), Ru1−H2 1.53(2), Ru1−H3 1.48(2), Ru1−C1 2.215(2), Ru1−C2 2.257(2), Ru1−C3 2.305(2), Ru1−C4 2.275(2), Ru1−C5 2.229(2), O1−H1b 1.25(3), H1b···N1 1.29(3), O3−H3b 0.82(3), O2···H3b 1.81(3), H1···H2 1.48, H1···H3 1.62; P1−Ru1−H2 76.0(9), P1−Ru1−H1 89.2(9), P1−Ru1−H3 76.1(9), H1−Ru1−H2 57.5(12), H1−Ru1−H3 64.4(12), H2−Ru1−H3 114.7(12), O1−H1b···N1 176(2), O3−H3b···O2 149(3).

mol^{-1}) than $\mathbf{2a_m \cdot indole^{H1}}$. Including entropic effects of the solute, the relative stabilities of the three adducts get closer: $\mathbf{2a_m \cdot indole^{NH}}$ and $\mathbf{2a_m \cdot indole^{H2}}$ are only 3.1 and 6.5 kJ mol^{-1} above $\mathbf{2a_m \cdot indole^{H1}}$ when ΔG_{DCM} are compared. Calculations indicate that the interaction of the weak proton donor with the nitrogen atom of the P,N ligand and with the hydride (in a bifurcated mode) should be of similar strength, making the equilibrium schematized in Chart 1 possible.

We have analyzed the influence of the hydrogen-bonding interaction with indole in the $H_{lateral}-H_{central}$ exchange responsible for QEC. The two most stable minima ($\mathbf{2a_m \cdot indole^{NH}}$ and $\mathbf{2a_m \cdot indole^{H1}}$) have been taken as starting points. The two transition states corresponding to the hydrogen exchange with the trihydride interacting with the indole are shown in Figure 7 (bottom). In both cases, the presence of the indole leads to a decrease on the Gibbs energy of activation for the hydrogen exchange, which is reduced from 63 kJ mol^{-1} when the proton donor is absent to 59.7 and 53.3 kJ mol^{-1} when it is placed in the *N*-pyridyl side ($\mathbf{TS_{Hexch} \cdot indole^{NH}}$) and the hydride side ($\mathbf{TS_{Hexch} \cdot indole^{H1}}$), respectively. This effect can be explained by reduction of the electronic density on the metal atom induced by interaction with the proton donor. This reduction stabilizes the dihydrogen species (transition state for the hydrogen exchange) and thus lowers the exchange barrier. The same phenomenon has been experimentally

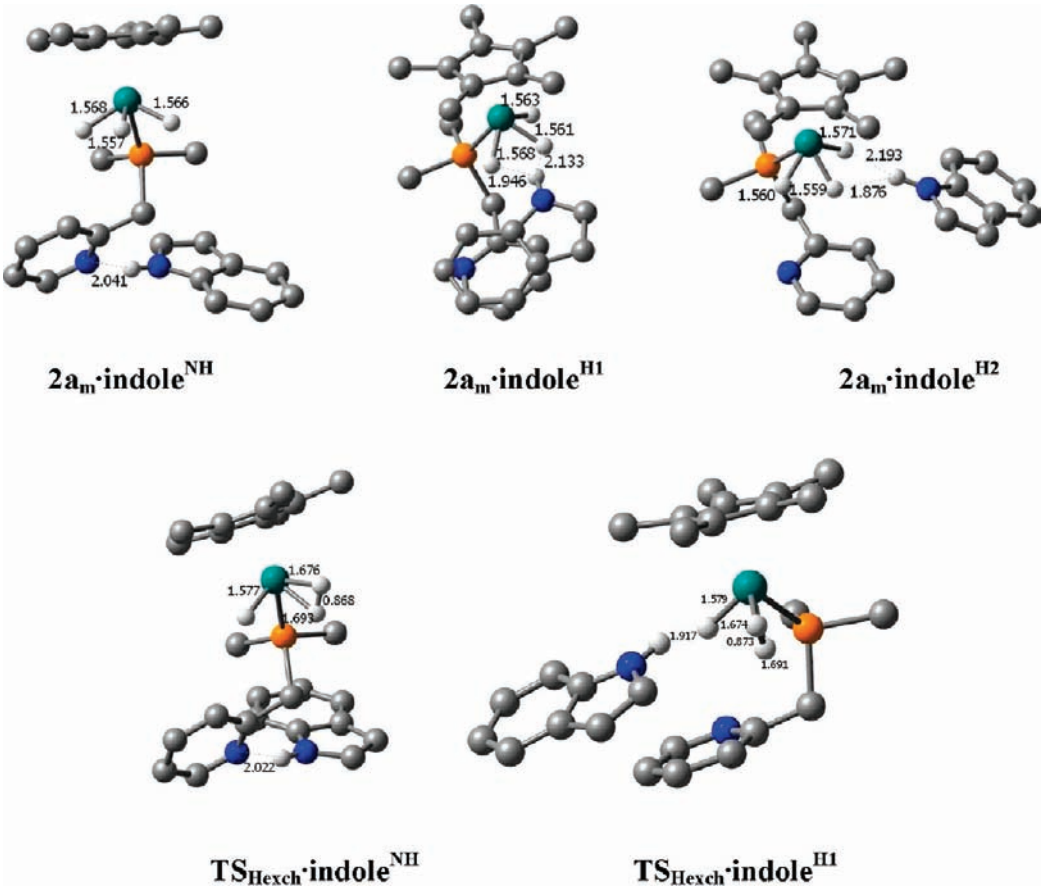

Figure 7. Optimized geometries of the hydrogen-bonded adducts of $\mathbf{2a_m}$ with indole (top) and transition states for hydrogen exchange (bottom). Hydrogen atoms except hydrides, dihydrogen, and indole protons have been omitted.

observed and theoretically analyzed for QEC in adducts of trihydride metallocenes with Lewis acids.[35] The reduction of the electron density on ruthenium is more pronounced when indole is interacting with hydride because it is directly bonded to the metal. The lower the exchange barrier the greater the exchange coupling should be in agreement with the experimental results (Table 1). From the lowering in $\Delta G^{\ddagger}_{exch}$ pointed out by the calculations, it is not possible to discriminate between the two indole adducts because both hydrogen bonding with the nitrogen atom and interaction with the hydride ligand should increase the hydrogen-exchange coupling constants.

5. Reactions with CF_3SO_3H: Proton Transfer. 5.1. 1 equiv of Acid. Once we examined the interaction of the trihydride complexes **2a**/**2b** with weak proton donors, we studied the proton-transfer reactions using the strong acid CF_3SO_3H. As was done in the case of weak proton donors, the reactions of **2a**/**2b** with the 1:1 CF_3SO_3H complex/acid ratio in CD_2Cl_2 were monitored in the temperature range −80 to +25 °C (Figure 8).

The ^{1}H NMR spectrum of **2a**/**2b** upon the addition of 1 equiv of CF_3SO_3H showed at 193 K one rather broad multiplet in the hydride region, which indicates the occurrence of QEC in the system. The multiplet appears centered at −11.2 ppm and exhibits $(T_1)_{min}$ of 213 ms in the case of **2a** and 109 ms for **2b**. The acidic proton appears in the ^{1}H NMR spectra at 193 K as a very broad low-field resonance near 14 ppm. As the temperature rises, the hydride resonances get increasingly broad, until the spectra become featureless in both the hydride and the acidic proton regions at 243 K. The ^{31}P{^{1}H} NMR spectra at 183 K consist of one broad or very broad resonance centered at 98.8 ppm for **2a** ($\Delta\nu_{1/2}$ = 52 Hz) and at 98.6 ppm for **2b** ($\Delta\nu_{1/2}$ = 440 Hz). These broad resonances become sharper at higher temperatures, reaching respective half-widths of 16 Hz (**2a**) and 64 Hz (**2b**) at 273 K. The process is fully reversible. These spectral data suggest that the trihydrides **2a**/**2b** are protonated by CF_3SO_3H at the nitrogen atom of the pendant pyridine or quinoline group, furnishing the cationic species [Cp*RuH$_3$(κ^1-P-^{i}Pr$_2$PCH$_2$XH)]-[CF_3SO_3] [X = Py (**4a**), Quin (**4b**)], which most likely contain one dihydrogen bond between the NH and one of the hydride ligands.

At temperatures above 243 K, a new rather broad hydride resonance begins to appear in the ^{1}H NMR spectra (Figure 8). Likewise, new signals also appear in the ^{31}P{^{1}H} NMR spectra: one singlet at 84.5 ppm in the case of **2a** and one at 77.8 ppm in the case of **2b**. $(T_1)_{min}$ for the new hydride resonances are very short (10 and 11 ms, respectively, in each case) and consistent with the presence of a dihydrogen ligand. Furthermore, the acidic proton resonances disappear at 298 K, and the doublet for the CH_2 group of the pendant pyridine or quinoline is

(35) (a) Antiñolo, A.; Carrillo, F.; Fernández-Baeza, J.; Otero, A.; Fajardo, M.; Chaudret, B. *Inorg. Chem.* **1992**, *31*, 5156–5157. (b) Camanyes, S.; Maseras, F.; Moreno, M.; Lledós, A.; Lluch, J. M.; Bertrán, J. *Inorg. Chem.* **1998**, *37*, 2334–2339.

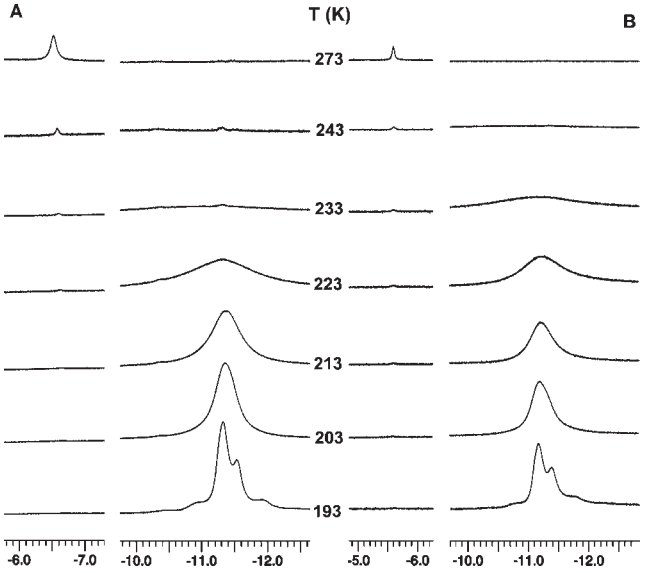

Figure 8. VT ^{1}H NMR (hydride region, 400 MHz) of samples made by the addition of 1 equiv of CF_3SO_3H to a frozen CD_2Cl_2 solution of **2a** (A) or **2b** (B), followed by subsequent warming to the indicated temperatures.

replaced by two multiplets corresponding to the AB part of an ABX spin system. The latter indicates a change in the coordination mode of the PN ligand from κ^1-P to chelating κ^2-P,N. We have identified these products as the cationic dihydrogen complexes $[Cp^*Ru(H_2)(\kappa^2\text{-P,N-}^i Pr_2PCH_2X)]^+$ [X = Py (**5a**), Quin (**5b**)]. The coupling constant $^1J_{HD}$ in these complexes was measured, having values of 28.4 Hz for **5a** and 28 Hz for **5b**. Chart 4 summarizes the species involved in the reaction of **2a**/**2b** with 1 equiv of CF_3SO_3H.

We have computationally studied the nature of the product obtained by protonation with 1 equiv of a strong acid. Optimization from different starting points by adding one proton to $\mathbf{2a_m}$ leads to three stable isomeric structures for the cationic species $\mathbf{4a_m}$ (Figure 9, top).

The most stable protonated product is $\mathbf{4a_m^{NH}}$ with the *N*-pyridyl protonated. Protonation of the central hydride gives structure $\mathbf{4a_m^{2HH2}}$ with one central dihydrogen and two lateral dihydride ligands. Protonation of both lateral hydrides gives the same bis(dihydrogen) product $\mathbf{4a_m^{2H2}}$. The stability of the two species arising from protonation of the trihydride unit is very similar. $\mathbf{4a_m^{NH}}$ is placed 20.6 and 19.6 kJ mol^{-1} below $\mathbf{4a_m^{2HH2}}$ and $\mathbf{4a_m^{2H2}}$, respectively. Interestingly, in $\mathbf{4a_m^{NH}}$, the pyridyl group has rotated in such a way that a strong dihydrogen bond is formed between the N-proton and two hydrides. This orientation could facilitate ulterior proton transfer to the hydride site.

In a low-polar solvent, ion-pair formation between the cationic protonation product and the triflate counteranion (OTf) can be expected. Ion pairing can affect both the thermodynamics of a reaction, by changing the relative energies of the species involved, and its kinetics and mechanisms, by providing alternative reaction pathways.[36] The ion-pair formation may become particularly important in proton-transfer reactions to transition-metal hydrides.[22,37,38] Thus, ion pairs of the three $\mathbf{4a_m}$ isomers with one triflate anion were optimized. The three stable isomeric structures are kept in the presence of the triflate counteranion (Figure 9, bottom). A hydrogen bond between one triflate oxygen atom and a protic hydrogen atom whether from the pyridyl group ($\mathbf{4a_m^{NH}\cdot OTf}$) or from the dihydrogen ligand ($\mathbf{4a_m^{2H2}\cdot OTf}$ and $\mathbf{4a_m^{2HH2}\cdot OTf}$) also contributes to the ion-pair stability. The energy ordering found without the counteranion is preserved when the triflate is included, with the stability of the N-protonated isomer being even increased with respect the hydride-protonated species. $\mathbf{4a_m^{NH}\cdot OTf}$ is placed 32.7 and 32.2 kJ mol^{-1} below $\mathbf{4a_m^{2HH2}\cdot OTf}$ and $\mathbf{4a_m^{2H2}\cdot OTf}$, respectively. $\mathbf{4a_m^{NH}\cdot OTf}$ is formed without a barrier when triflic acid is placed close to the nitrogen atom and it lies 55.5 kJ mol^{-1} below the separated reactants ($\mathbf{2a_m}$ and HSO_3CF_3), in agreement with a fast and easy protonation with triflic acid. Indeed, calculations support the initial protonation of the trihydride at the pendant pyridine or quinoline group, furnishing the cationic species **4a** and **4b**.

Protonation introduces a mobile hydrogen center in the coordination sphere of the transition metal, allowing the initial protonated intermediate to evolve in a variety of ways.[22] We have theoretically analyzed possible pathways for proton transfer from the pyridyl nitrogen atom to

Chart 4

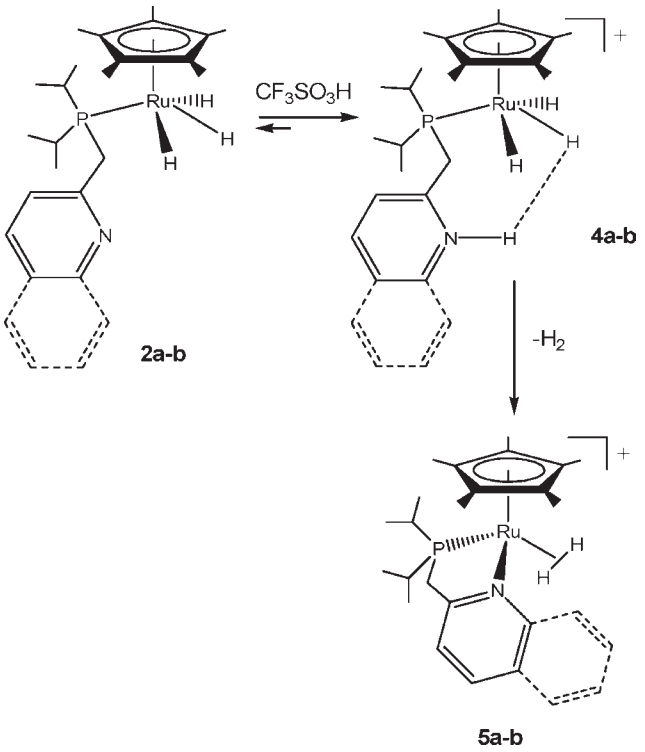

(36) (a) Macchioni, A. *Chem. Rev.* **2005**, *105*, 2039–2073. (b) Clot, E. *Eur. J. Inorg. Chem.* **2009**, 2319–2328.

(37) (a) Basallote, M. G.; Besora, M.; Durán, J.; Fernández Trujillo, M. J.; Lledós, A.; Máñez, M. A.; Maseras, F. *J. Am. Chem. Soc.* **2004**, *126*, 2320–2321. (b) Basallote, M. G.; Besora, M.; Castillo, C. E.; Fernández Trujillo, M. J.; Lledós, A.; Maseras, F.; Máñez, M. A. *J. Am. Chem. Soc.* **2007**, *129*, 6608–6618. (c) Algarra, A. G.; Fernandez Trujillo, M. J.; Lledós, A.; Basallote, M. G. *Chem. Commun.* **2009**, 4563–4565.

(38) (a) Kovács, G.; Ujaque, G.; Lledós, A. *J. Am. Chem. Soc.* **2008**, *130*, 853–864. (b) Xia, Y. Z.; Dudnik, A. S.; Gevorgyan, V; Li, Y. H. *J. Am. Chem. Soc.* **2008**, *130*, 6940–6941.

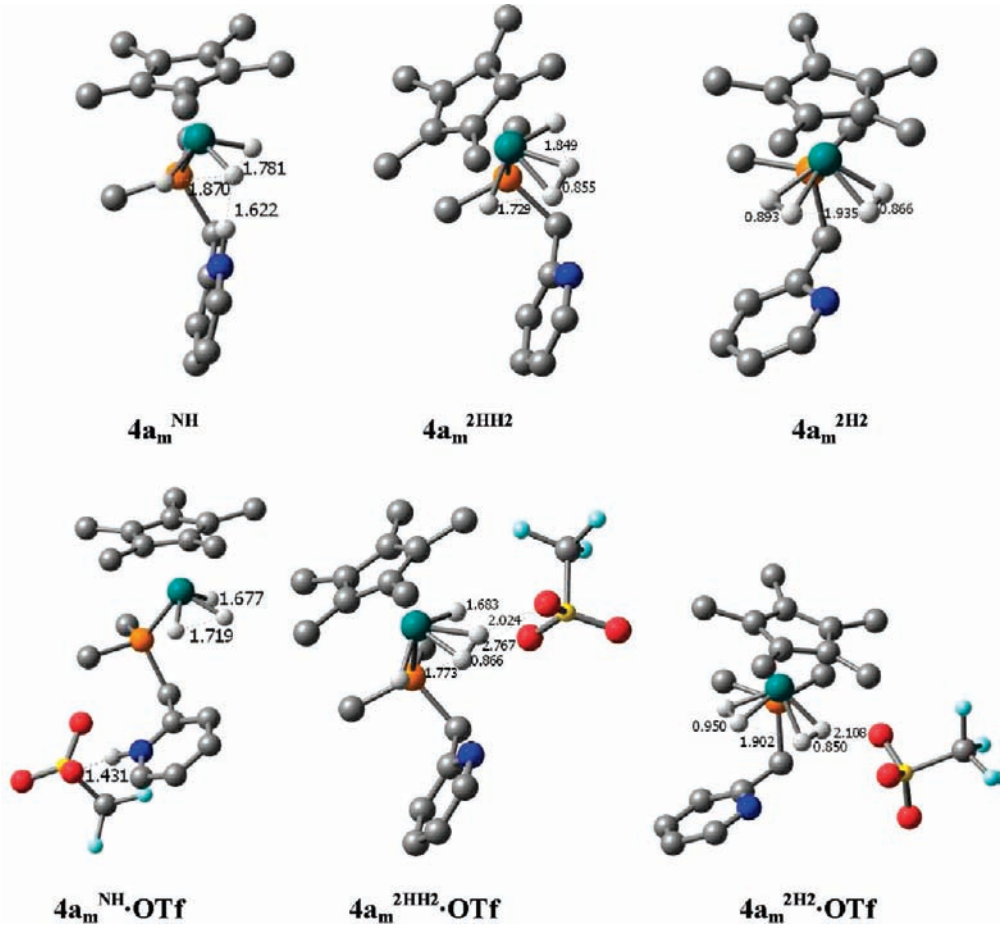

Figure 9. Optimized geometries of the isomers of the first protonation product ($\mathbf{4a_m}$) without (top) and with (botton) the triflate counteranion. Hydrogen atoms except hydrides, dihydrogen, or N-proton in the pyridyl have been omitted.

the trihydride unit. For the isolated cation, two transition states have been located for this process (Figure 10). One [**TS(NH-H$_{lat}$)**] corresponds to proton transfer to the lateral hydride and leads to the bis(dihydrogen) isomer $\mathbf{4a_m^{2H2}}$. The other one [**TS(NH-H$_{cent}$)**] describes protonation of the central hydride and gives the dihydrido(dihydrogen) isomer $\mathbf{4a_m^{2HH2}}$. In both transition states, the distance between the incoming proton and the closest hydride is about 1 Å, indicating that a dihydrogen unit has already been formed at the transition state. $\Delta G^{\ddagger}$ barriers of 47.0 and 45.2 kJ mol^{-1} are obtained for the formation of $\mathbf{4a_m^{2H2}}$ and $\mathbf{4a_m^{2HH2}}$ from $\mathbf{4a_m^{NH}}$, respectively.

It has been shown that triflate anions can behave as a proton shuttle, facilitating proton transfer.[38] Separated $\mathbf{2a_m}$ and triflic acid are only 55.5 kJ mol^{-1} above the most stable ($\mathbf{4a_m}$, triflate) ion pair. Then the triflic acid can protonate either a lateral or central hydride of the trihydride, leading to the bis(dihydrogen) (**$\mathbf{4a_m^{2H2}}$·OTf**) and dihydrido(dihydrogen) (**$\mathbf{4a_m^{2HH2}}$·OTf**) ion pairs. The transition states for both proton transfers have been located and are depicted in Figure 10 (bottom). The transition state corresponding to the protonation of a central hydride [**TS(HOTf-H$_{cent}$)**] lies only 5.2 kJ mol^{-1} above $\mathbf{2a_m}$ + HOTf, being a bit lower than that of the lateral hydride protonation [**TS(HOTf-H$_{lat}$)**, 17.2 kJ mol^{-1} above $\mathbf{2a_m}$ + HOTf].

Overall calculations agree with a very easy initial protonation of the *N*-pyridyl by the triflic acid, followed when heating by proton transfer to the hydride site with the formation of one or two dihydrogen ligands. The triflate counteranion can assist the proton migration, acting as a proton shuttle. Ulterior dihydrogen elimination could displace the protonation reaction toward the dihydrogen complex formation.

5.2. Excess of Acid: Second Protonation. We have also studied the proton-transfer reactions to **2a**/**2b** in CD_2Cl_2 using an excess (3 equiv) of CF_3SO_3H in the temperature range 193−298 K. Under these conditions, at 193 K, a new broad resonance appears in the hydride region of the ^{1}H NMR spectrum at −8.1 ppm in the case of **2a** (Figure 11).

This new resonance has a $(T_1)_{min}$ of 13.9 ms. The $^{31}P\{^1H\}$ NMR spectrum at the same temperature displays one singlet at 79.9 ppm. In analogous fashion, the ^{1}H NMR spectrum of **2b** with an excess of CF_3SO_3H added showed at 193 K one broad signal at −7.95 ppm having a $(T_1)_{min}$ of 12.4 ms (Figure 11B) and one singlet at 80.4 ppm in the $^{31}P\{^1H\}$ NMR spectrum. At this temperature, a small amount of the respective dihydrogen complexes **5a**/**5b** is already present as inferred from the ^{1}H and $^{31}P\{^1H\}$ NMR spectra. As the temperature increases, the broad hydridic resonances near −8 ppm decrease their intensity at the expense of the signals for the dihydrogen ligand in **5a**/**5b**. At 273 K, the dihydrogen complex **5a** or **5b** becomes predominant. The short $(T_1)_{min}$ measured for the new hydridic signals near −8 ppm indicates clearly the

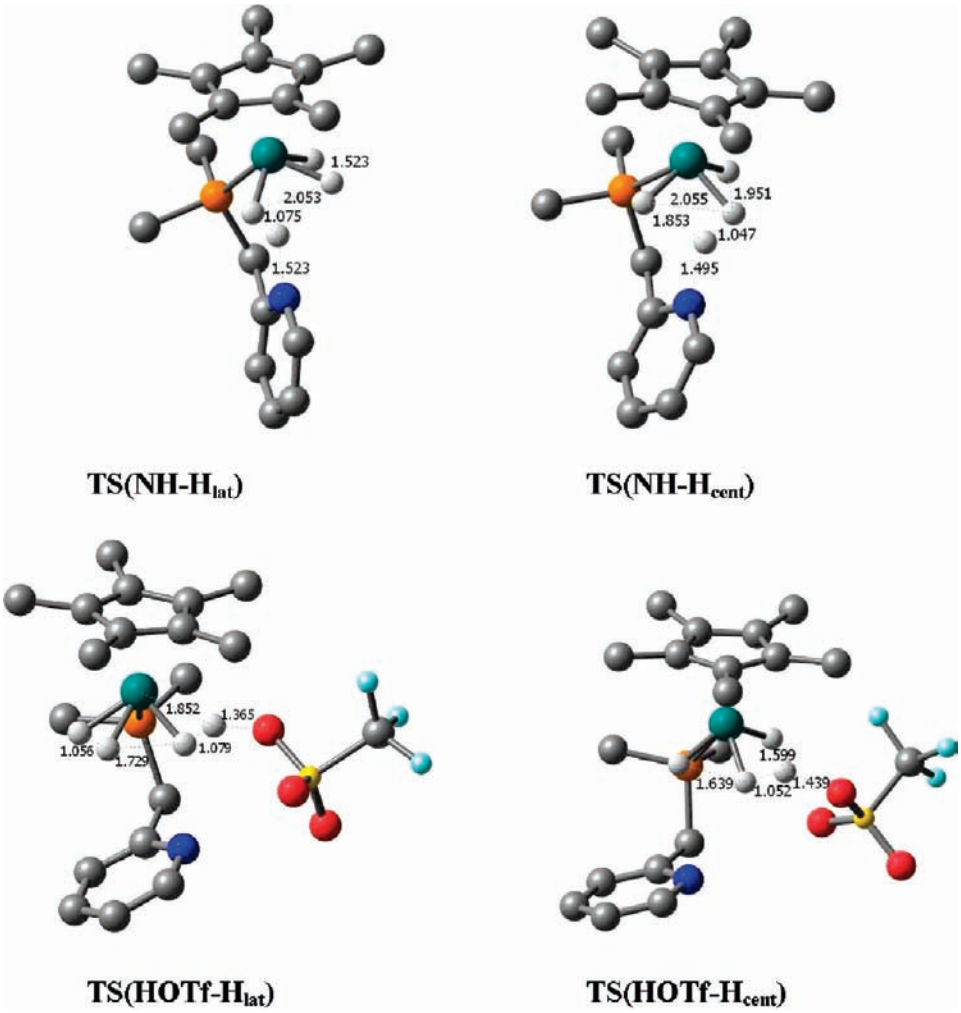

Figure 10. Transition states of intramolecular proton transfer from the pyridyl nitrogen atom to the trihydride unit (top) and of trihydride protonation by triflic acid (bottom). Hydrogen atoms except hydrides, dihydrogen, or N-proton in the pyridyl have been omitted.

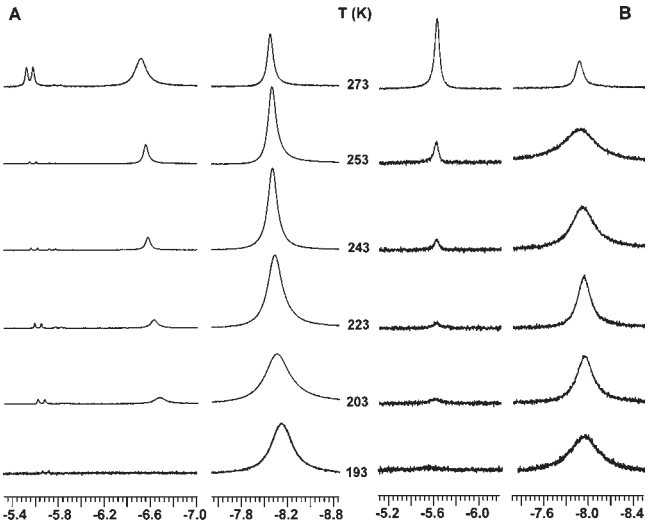

Figure 11. VT ^{1}H NMR (hydride region, 400 MHz) spectra of samples made by the addition of an excess (3 equiv) of CF_3SO_3H to a frozen CD_2Cl_2 solution of **2a** (A) or **2b** (B), followed by subsequent warming to the indicated temperatures.

presence of dihydrogen ligands. We attribute resonances to the dicationic complexes [Cp*RuH$_4$(κ^1-P-^{i}Pr$_2$PCH$_2$XH)]$^{2+}$ [X = Py (**6a**), Quin (**6b**)], resulting from a second protonation of **4a**/**4b** at the hydride site. These species can be formulated either as bis(dihydrogen) complexes [Cp*Ru(H$_2$)$_2$(κ^1-P-^{i}Pr$_2$PCH$_2$XH)]$^{2+}$ (X = Py, Quin) or as dihydrido(dihydrogen) species [Cp*RuH$_2$(H$_2$)(κ^1-P-^{i}Pr$_2$PCH$_2$XH)]$^{2+}$. We have previously described the bis(dihydrogen) complexes [Cp*Ru(H$_2$)$_2$(EPh$_3$)]$^+$ (E = As, Sb),[6] generated by protonation of the corresponding [Cp*RuH$_3$(EPh$_3$)] derivatives. These bis(dihydrogen) complexes were stable up to 273 K and were characterized in solution by T_1 and $^1J_{HD}$ measurements. $(T_1)_{min}$ measured for the hydride resonances of the dicationic species [Cp*RuH$_4$(κ^1-P-^{i}Pr$_2$PCH$_2$XH)]$^{2+}$ (13.9 ms for **6a** and 12.4 ms for **6b**) are short and comparable to those of the dihydrogen resonances in **5a**/**5b** and in [Cp*Ru(H$_2$)$_2$(EPh$_3$)]$^+$ (E = As, Sb).[6] A dihydrido(dihydrogen) structure has been postulated for the related species [Cp*RuH$_4$(PCy$_3$)]$^+$ [$(T_1)_{min}$ = 18 ms at 500 MHz], although a bis(dihydrogen) structure was not ruled out in this case.[18] The two recently reported bis(dihydrogen) osmium derivatives [TpOs(H$_2$)$_2$(P^{i}Pr$_3$)][BF$_4$][39] and [Os(BAEA)(H$_2$)$_2$(P^{i}Pr$_3$)][BF$_4$]$_2$ [BAEA = bis(2-aminoethyl)amine][40] display $(T_1)_{min}$ values of 12 and

(39) Castro-Rodrigo, R.; Esteruelas, M. A.; López, A. M.; Oliván, M.; Oñate, E. *Organometallics* **2007**, *26*, 4498–4509.
(40) Baya, M.; Esteruelas, M. A.; Oliván, M.; Oñate, E. *Inorg. Chem.* **2009**, *48*, 2677–2686.

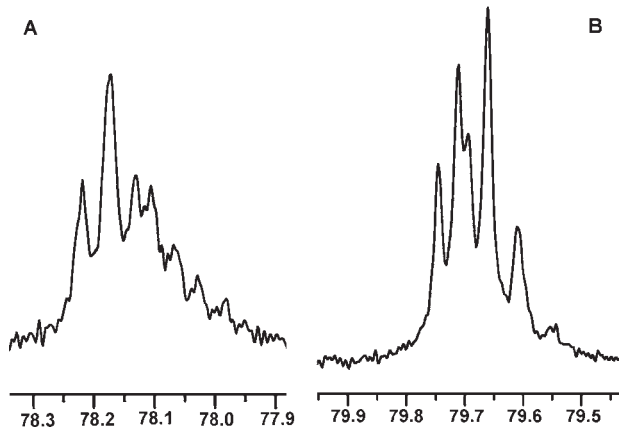

Figure 12. $^{31}P\{^1H\}$ NMR spectra of samples made by the addition of an excess of CF_3SO_3D (3 equiv) to a frozen CD_2Cl_2 solution of **2a** (A) or **2b** (B), followed by subsequent warming to 233 K.

14 ms, respectively. On the other hand, the also related half-sandwich dihydride(dihydrogen)osmium complex $[Cp^*OsH_2(H_2)(PPh_3)][BF_4]$ (structure determined by neutron diffraction) shows in its ^1H NMR spectrum a single hydride resonance with a $(T_1)_{min}$ of 79.2 ms at 400 MHz (99 ms at 500 MHz) due to rapid scrambling between dihydride and dihydrogen sites.[41] A comparison of all of these data with ours suggests that **6a**/**6b** can be better formulated as the bis(dihydrogen) complexes $[Cp^*Ru(H_2)_2(\kappa^1\text{-P-}^iPr_2PCH_2XH)]^{2+}$ (X = Py, Quin). In order to confirm this, we attempted to measure $^1J_{HD}$ in any of the possible isotopomers of $[Cp^*RuH_nD_{4-n}(\kappa^1\text{-P-}^iPr_2PCH_2XD)]^{2+}$ (n = 1−3) by performing the reaction of **2a**/**2b** with an excess (3 equiv) of CF_3SO_3D. The hydride resonances in the ^1H NMR spectra were broad and unresolved and did not show any measurable H−D coupling. However, the $^{31}P\{^1H\}$ NMR spectra did show coupling of phosphorus−deuterium in the form of overlapping multiplets due to mixtures of isotopomers (Figure 12).

This is a feature more typical of terminal hydride (or deuteride) ligands attached to ruthenium. Thus, whereas the short $(T_1)_{min}$ point to a bis(dihydrogen) structure, the failure to observe $^1J_{HD}$ and the occurrence of phosphorus−deuterium couplings suggests that terminal hydride ligands are also present in the system. We must therefore assume that the dicationic species $[Cp^*RuH_4(\kappa^1\text{-P-}^iPr_2PCH_2XH)]^{2+}$ exist in solution as equilibrium mixtures of both dihydride(dihydrogen) and bis(dihydrogen) tautomers. Additionally, the rapid exchange of the NH proton with the hydride and/or the hydrogen atoms of the dihydrogen ligands also occurs in this system.

6a and **6b** are acidic and exist in equilibrium with the corresponding monoprotonated species **4a**/**4b**. As the temperature increases, the equilibrium shifts to the monoprotonated species, which undergo irreversible dihydrogen elimination and transformation into the mono(dihydrogen) complexes **5a**/**5b**. At temperatures above 273 K, the dicationic species disappear completely. The relationships among the species involved in the protonation reactions of **2a**/**2b** with an excess of CF_3SO_3H are summarized in Chart 5.

Chart 5

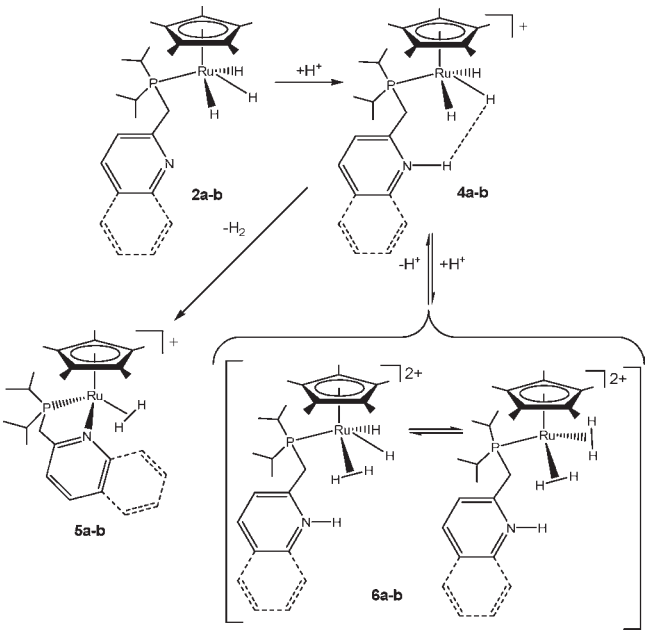

In the case of **2a** plus an excess of CF_3SO_3H, apart from the signal for the dihydrogen complex **5a**, one hydridic doublet resonance also appears at −5.55 ppm at 273 K (Figure 11A). At 298 K, this doublet becomes one broad unresolved signal. It corresponds to a species that displays one singlet at 92.3 ppm in the $^{31}P\{^1H\}$ NMR spectrum. A new resonance also appears in the ^{19}F NMR spectrum at −78.6 ppm. We have rationalized these observations by considering the formation of the ruthenium(IV) species $[Cp^*RuH(CF_3SO_3)(\kappa^2\text{-P,N-}^iPr_2PCH_2Py)][CF_3SO_3]$ (**7a**), formally derived from the oxidative addition of a CF_3SO_3H molecule to the coordinatively unsaturated complex $[Cp^*Ru(\kappa^2\text{-P,N-}^iPr_2PCH_2Py)]^+$ (**10a**, vide infra).

Solutions of **7a** for the NMR study were easily obtained by treating **2a** with 2 equiv of CF_3SO_3H in CD_2Cl_2 under argon. The resonance of the C5 ring for **7a** appears at 103.26 ppm in the $^{13}C\{^1H\}$ NMR spectrum, a value that is consistent with the formulation as a formally seven-coordinate ruthenium(IV) species.[42] Attempts made to isolate **7a** as a solid were only partially successful. An orange solid was obtained by the addition of petroleum ether to acidic solutions of **7a** in DCM. However, this solid always converted to a sticky material when isolated and washed. For this reason, it was not analyzed.

We have theoretically addressed the nature of the diprotonated species. From the most stable monoprotonated product $\mathbf{4a_m}^{\mathbf{NH}}$, three protonation sites are available, corresponding to the three hydrides. Four different minima have been found for the dicationic species $\mathbf{6a_m}$. Three of them are dihydrogen−dihydride species, differing in the relative position of the dihydrogen ligand, central in $\mathbf{6a_m}^{\mathbf{HH2H}}$ and lateral in $\mathbf{6a_m}^{\mathbf{HHH2}}$ and $\mathbf{6a_m}^{\mathbf{H2HH}}$. The fourth has two dihydrogen ligands ($\mathbf{6a_m}^{\mathbf{2H2}}$; Figure 13).

The four isomers have very similar stabilities. The most stable complex is the bis(dihydrogen) structure $\mathbf{6a_m}^{\mathbf{2H2}}$,

(41) Gross, C. L.; Young, D. M.; Schultz, A. J.; Girolami, G. *J. Chem. Soc., Dalton Trans.* **1997**, 3081–3082.

(42) Aneetha, H.; Jiménez-Tenorio, M.; Puerta, M. C.; Valerga, P.; Sapunov, V. N.; Schmid, R.; Kirchner, K.; Mereiter, K. *Organometallics* **2002**, *21*, 5334–5346.

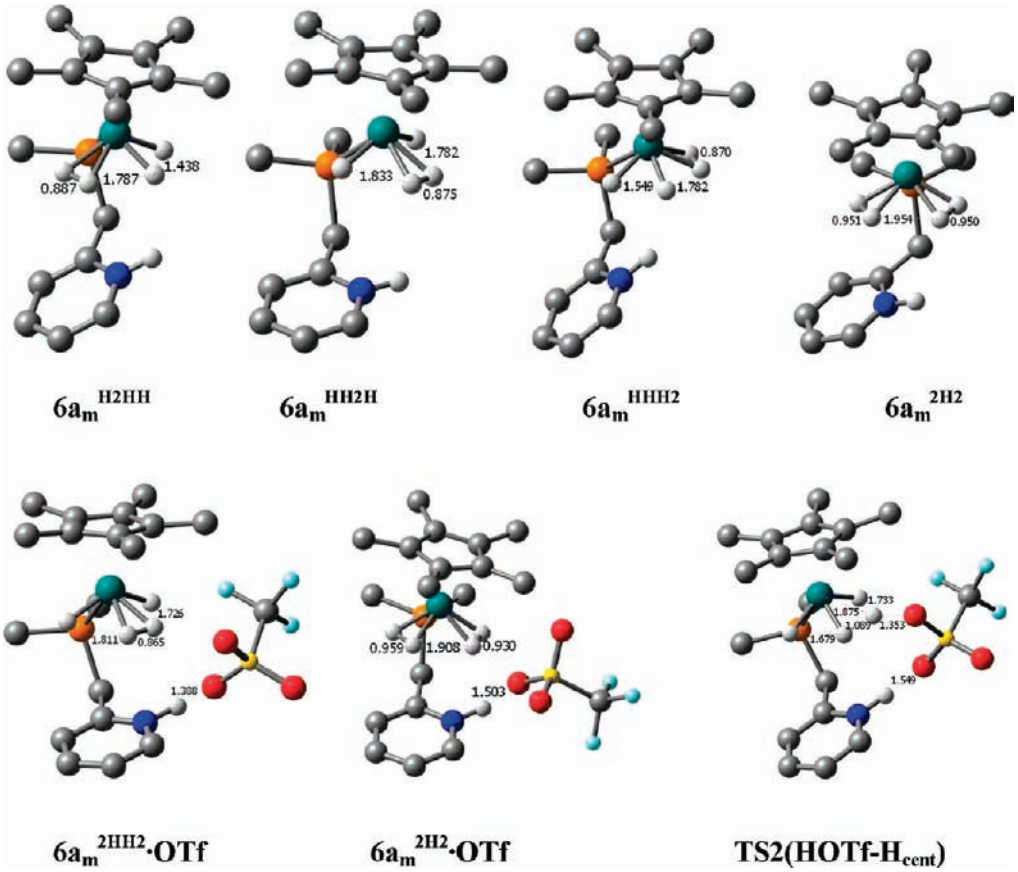

Figure 13. Optimized geometries of isomers of the product of the second protonation $\mathbf{6a_m}$ without (top) and with (bottom) the triflate counteranion and the transition state of the protonation. Hydrogen atoms except hydrides, dihydrogen, or N-proton in the pyridyl have been omitted.

but $\mathbf{6a_m}^{\mathbf{HH2H}}$, $\mathbf{6a_m}^{\mathbf{H2HH}}$, and $\mathbf{6a_m}^{\mathbf{HHH2}}$ are only 9.6, 4.0, and 10.4 kJ mol^{-1} above the bis(dihydrogen) dication, respectively. From these values and the proximity of the hydrogen ligands, a fast interconversion between the bis(dihydrogen) and dihydride(dihydrogen) structures can be envisaged.[9] The second protonation is less favored than the first one. Formation of the most stable diprotonated isomer ($\mathbf{6a_m}^{\mathbf{2H2}}$) from the most stable monoprotonated compound ($\mathbf{4a_m}^{\mathbf{NH}}$) is an endergonic process, with the diprotonated species being 6.8 kJ mol^{-1} less stable than the monoprotonated one.

In the presence of triflate, two different ion pairs have been found as minima: the bis(dihydrogen) $\mathbf{6a_m}^{\mathbf{2H2}}\cdot\mathbf{OTf}$ and one dihydride(dihydrogen) with the dihydrogen ligand at the central position ($\mathbf{6a_m}^{\mathbf{2HH2}}\cdot\mathbf{OTf}$; Figure 13). The bis(dihydrogen) remains as the most stable structure, but only 5.9 kJ mol^{-1} below the dihydride(dihydrogen) isomer. Kinetically, the second protonation is favored. The transition state corresponding to the protonation of a central hydride [$\mathbf{TS2(HOTf\text{-}H_{cent})}$] lies only 9.2 kJ mol^{-1} above $\mathbf{4a_m}^{\mathbf{NH}}$ + HOTf .

We have also theoretically addressed the feasibility of the formation of ruthenium(IV) species [Cp*RuH(CF_3SO_3)-(κ^2-P,N-^{i}Pr$_2$PCH$_2$Py)][CF_3SO_3] (**7a**; Chart 6). $\mathbf{7a_m}$ (Figure 14) is a stable species, more stable than both the dihydrogen complex $\mathbf{5a_m}$ (13.1 kJ mol^{-1} below) and the unsaturated complex $\mathbf{10a_m}$ (53.2 kJ mol^{-1} below). Calculations do support the formation of **7a**.

5.3. Computational Study of Dihydrogen Elimination. The experimental study shows that, upon an increase in the temperature, the protonated structures **4** can evolve by eliminating dihydrogen, with a subsequent change in the coordination mode of the P,N ligand from κ^1-P to chelating κ^2-P,N.

The dihydrogen elimination from the two isomers of $\mathbf{4a_m}$ bearing dihydrogen ligands has been examined. Dihydrogen elimination from the bis(dihydrogen) $\mathbf{4a_m}^{\mathbf{2H2}}$ leads to the dihydrogen complex $\mathbf{5a_m}$ with a Gibbs energy barrier of 70.0 kJ mol^{-1}. The process from the dihydride(dihydrogen) isomer $\mathbf{4a_m}^{\mathbf{2HH2}}$ leads to the dihydride $\mathbf{5a_m}^{\mathbf{2H}}$, 19.6 kJ mol^{-1} less stable than the dihydrogen, after crossing a Gibbs energy barrier of 81.1 kJ mol^{-1}. Kinetics and thermodynamics both lead to the dihydrogen $\mathbf{5a_m}$. The two located transition states are collected in Figure 15. Their structures show that in addition to the elimination of one dihydrogen unit the change of the coordination mode of the P,N ligand from κ^1-P to chelating κ^2-P,N is also taking place.

6. Isolation and Structure of 5a/5b and Related Compounds. The dihydrogen complexes **5a** and **5b** were isolated in the form of yellow crystalline materials by the reaction of **1a** or **1b** with dihydrogen and NaBAr′$_4$ [Ar′$_4$ = 3,5-C$_6$H$_3$(CF$_3$)$_2$] in diethyl ether. These compounds are stable both in the solid state and in solution under a hydrogen atmosphere. Remarkably, these compounds do not undergo irreversible isomerization to the corresponding ruthenium(IV) dihydride complexes at 298 K. This fact contrasts with the behavior commonly observed for half-sandwich ruthenium dihydrogen derivatives.[43,44] On the other hand, the stability of the dihydrogen isomer

Chart 6

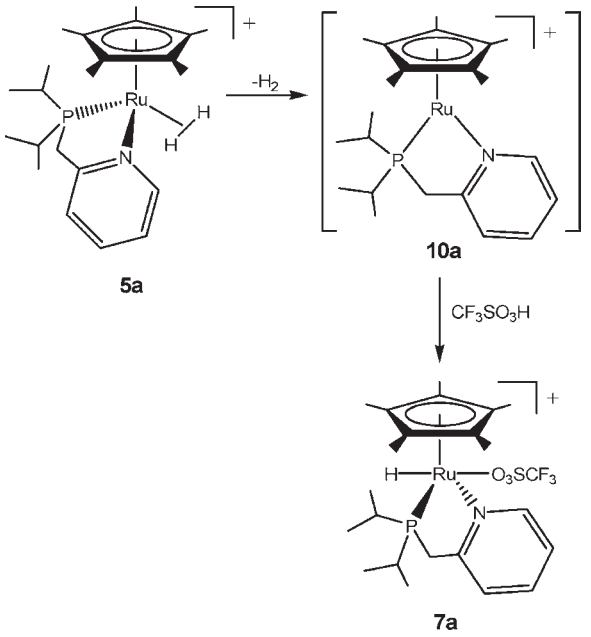

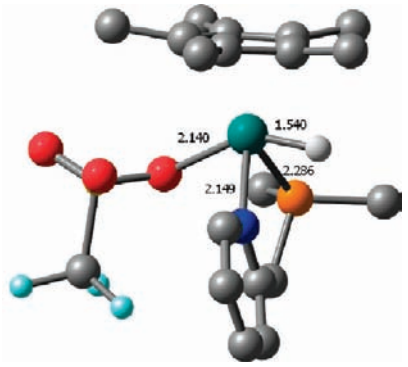

Figure 14. Optimized geometry of the product $\mathbf{7a_m}$. Hydrogen atoms except hydride have been omitted.

versus the dihydride isomer for **5a** and **5b** resembles the analogue properties of hydrotris(pyrazolyl)borate (Tp) ruthenium dihydrogen complexes $[TpRu(H_2)P_2]^+$ [P_2 = 1,2-bis(diisopropylphosphino)ethane,[45] 1,2-bis(diisopropylphosphinoamino)ethane, 1,2-bis(diisopropylphosphinoamino)cyclohexane].[46]

Single crystals of **5b** were obtained by the slow diffusion of petroleum ether through a diethyl ether solution of the complex under dihydrogen. The resulting large yellow crystals were subjected to X-ray structure analysis. An ORTEP view of the complex cation $[Cp^*Ru(H_2)(\kappa^2\text{-}P,N\text{-}^iPr_2PCH_2Quin)]^+$ in **5b** is shown in Figure 16, together with the most relevant bond distances and angles.

As far as we are aware, the only other half-sandwich dihydrogen complex of ruthenium that has been structu-

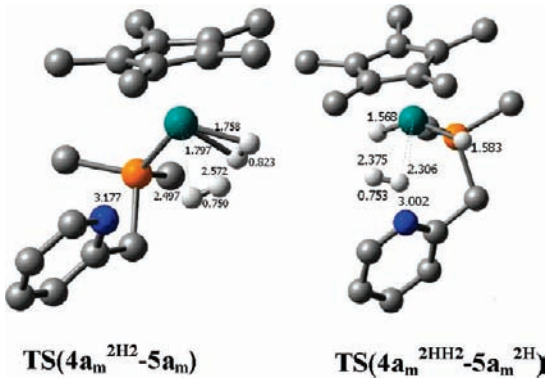

Figure 15. Transition states for the dihydrogen elimination from $\mathbf{4a_m}^{2H2}$ [$\mathbf{TS(4a_m}^{2H2}\mathbf{\text{-}5a_m)}$, left] and from $\mathbf{4a_m}^{2HH2}$ [$\mathbf{TS(4a_m}^{2HH2}\mathbf{\text{-}5a_m}^{2H})$, right]. Hydrogen atoms except hydrides or dihydrogen have been omitted.

rally characterized is $[Cp^*Ru(H\cdots H)(dppm)][BF_4]$,[47,48] which contains an elongated dihydrogen ligand.[49] The dihydrogen ligand in this compound was not localized in an initial X-ray crystallography structure analysis.[47] However, a subsequent neutron diffraction study revealed the position and dimensions of the elongated dihydrogen ligand.[48] The complex cation $[Cp^*Ru(H_2)(\kappa^2\text{-}P,N\text{-}^iPr_2PCH_2Py)]^+$ adopts a "three-legged-piano-stool" structure. The conformation of the Ru1−P1−C20−C11−N1 ring is similar to that found in the structure of **1b**. The dihydrogen ligand was located and refined. The Ru1−H1 and Ru1−H2 bond lengths have values of 1.69(5) and 1.66(5) Å, respectively, which compare well with the values found in $[TpRu(H_2)(^iPr_2PNHCH_2CH_2NHP^iPr_2)][BAr'_4]$ by X-ray crystallography [1.685(19) and 1.66(4) Å][46] and in $[Cp^*Ru(H\cdots H)(dppm)][BF_4]$ by neutron diffraction [1.66(2) and 1.67(2) Å].[48] The H1−H2 bond distance of 0.67(6) Å is also comparable to the value of 0.69(4) Å reported for $[TpRu(H_2)(^iPr_2PNHCH_2CH_2NHP^iPr_2)][BAr'_4]$[46] but much shorter than the H1···H2 separation of 1.08(3) Å in $[Cp^*Ru(H\cdots H)(dppm)][BF_4]$.[48] Even considering the experimental error in the determination of these structural parameters by X-ray crystallography, the results are fully consistent with the presence of one dihydrogen molecule bound in a side-on manner to the ruthenium atom.

Quantum-mechanical calculations have proven to be a cost-effective high-quality technique for the precise location of the positions of hydrogen atoms in transition-metal complexes.[9] In order to refine the position of the dihydrogen ligand in complex **5b**, we fully optimized the geometry of the real complex. The optimized structure is depicted in Figure 17, together with that of the model complex $\mathbf{5a_m}$, and a comparison of the calculated parameters with the X-ray determined and with those of $\mathbf{5a_m}$ can be found in the Supporting Information (Table 1S). Bond distances and angles for the non-hydrogen atoms are in excellent agreement with the X-ray structure.

The $Ru-H_2$ unit presents a very similar arrangement in the model complex $\mathbf{5a_m}$ and in **5b**, with Ru−H and H−H

(43) Morris, R. H. *Coord. Chem. Rev.* **2008**, *252*, 2381–2394.
(44) Jimenez-Tenorio, M.; Palacios, M. D.; Puerta, M. C.; Valerga, P. *Inorg. Chem.* **2007**, *46*, 1001–1012.
(45) Jiménez-Tenorio, M. A.; Jiménez-Tenorio, M.; Puerta, M. C.; Valerga, P. *Inorg. Chim. Acta* **1997**, *259*, 77–84.
(46) Jiménez-Tenorio, M.; Palacios, M. D.; Puerta, M. C.; Valerga, P. *Organometallics* **2005**, *24*, 3088–3098.
(47) Jia, G.; Lough, A. J.; Morris, R. H. *Organometallics* **1992**, *11*, 161–171.
(48) Klooster, W. T.; Koetzle, T. F.; Jia, G.; Fong, T. P.; Morris, R. H.; Albinati, A. *J. Am. Chem. Soc.* **1994**, *116*, 7677–7681.
(49) (a) Gelabert, R.; Moreno, M.; Lluch, J. M.; Lledós, A. *J. Am. Chem. Soc.* **1997**, *119*, 9840–9847. (b) Heinekey, D. M.; Lledós, A.; Lluch, J. M. *Chem. Soc. Rev.* **2004**, *33*, 175–182.

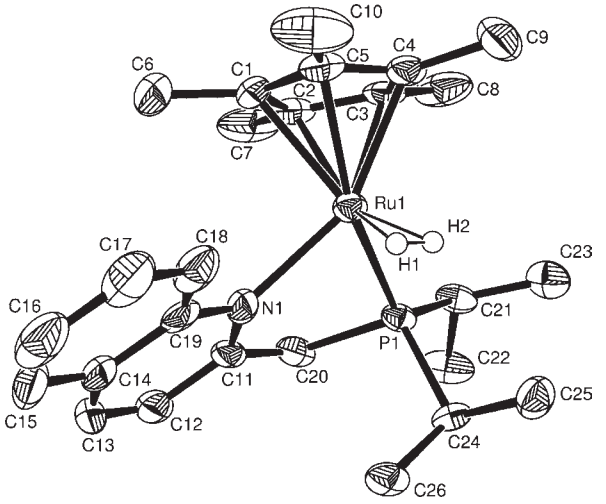

Figure 16. ORTEP drawing (50% thermal ellipsoids) of the cation $[Cp^*Ru(H_2)(\kappa^2\text{-}N,P\text{-}^iPr_2PCH_2Quin)]^+$ in complex **5b**. Hydrogen atoms except dihydrogen have been omitted. Selected bond lengths (Å) and angles (deg) with estimated standard deviations in parentheses: Ru1−P1 2.2902(13), Ru1−N1 2.173(4), Ru1−H1 1.69(5), Ru1−H2 1.66(5), Ru1−C1 2.231(5), Ru1−C2 2.183(4), Ru1−C3 2.203(4), Ru1−C4 2.185(5), Ru1−C5 2.232(5), H1−H2 0.67(6); P1−Ru1−N1 78.30(11), H1−Ru1−H2 22.9(19).

distances of about 1.64 and 0.95 Å, respectively. The H−H distance indicates a somewhat activated dihydrogen ligand, although less than that in the elongated dihydrogen ligand of $[Cp^*Ru(H\cdots H)(dppm)]^+$.[47−49] The dihydrogen dissociation energies are also very similar in both compounds (81.9 kJ mol^{-1} in $\mathbf{5a_m}$ and 82.7 kJ mol^{-1} in **5b**). The apparent disagreement between the calculated H−H separation in **5b** and the distance obtained by X-ray crystallography [0.67(6) Å] can be attributed to the intrinsic limitations of this technique for the accurate determination of bond distances involving hydrogen atoms, as well as the fact that the measurements correspond to the solid state. We have determined the H−H bond distances in a CD_2Cl_2 solution based upon $(T_1)_{min}$ (eq 1) and $^1J_{HD}$ coupling constants (eq 2).[6]

$$r_{H\cdots H} = 5.815[(T_1)_{min}/\nu]^{1/6} \quad (1)$$

$$r_{H\cdots H} = 1.42 - 0.0167(^1J_{HD}) \quad (2)$$

ν in eq 1 represents the NMR frequency of operation, which in our case is 4×10^8 Hz. The resulting H−H bond distances for **5b** using eqs 1 and 2 are respectively 1.01 and 0.95 Å. Both values are in much better agreement, with the H−H separations derived from DFT calculations. For compound **5a**, the corresponding H−H bond distances obtained by the application of eqs 1 and 2 are 0.99 and 0.95 Å, respectively.

In contrast with the behavior commonly found for the half-sandwich ruthenium dihydrogen derivatives, isomerization to the corresponding dihydride complexes has not been observed for compounds **5a** and **5b**. In $[(C_5R_5)\text{-}RuL_2H_2]^+$ species systems, the only stable dihydride is the *trans*-dihydride; thus, the dihydrogen−dihydride interconversion implies an important stereochemical change, passing from the three-legged-piano-stool dihydrogen complex to a transoid square-based four-legged-piano-stool dihydride. The optimized geometries of the *trans*-dihydride $\mathbf{5a_m}^{\mathbf{2H}}$ and the transition state for the interconversion are shown in Figure 18.

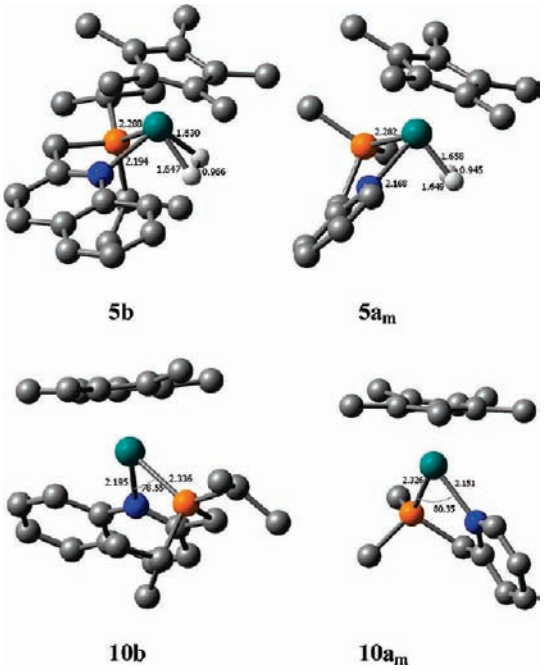

Figure 17. Optimized geometries of the dihydrogen complexes **5b** and $\mathbf{5a_m}$ and the corresponding 16-electron species (**10b** and $\mathbf{10a_m}$).

The transition state for the rearrangement [**TS(H2-HH)**], depicted in Figure 18, has a dihydride nature (Ru−H bond distances of 1.574 and 1.583 Å), with no interaction between the two hydrogen atoms (distance H−H of 2.408 Å). The geometry around the ruthenium atom in this transition state is similar to that reported for the dihydrogen → *trans*-dihydride isomerization in related half-sandwich complexes.[50] In this system, the dihydride is 19.6 kJ mol^{-1} less stable than the dihydrogen. Moreover, $\Delta G^{\ddagger}$ for the isomerization (99.1 kJ mol^{-1}) is considerably higher than that for the dihydrogen elimination (40.1 kJ mol^{-1}). Both thermodynamics and kinetics favor dihydrogen elimination from $\mathbf{5a_m}$, giving the unsaturated complex $\mathbf{10a_m}$, in front of the oxidative addition that leads to the dihydride $\mathbf{5a_m}^{\mathbf{2H}}$. Indeed, this is the experimental behavior observed in complexes **5a** and **5b**.

The dihydrogen ligand in **5a** and **5b** is extremely labile and readily replaced by dinitrogen in DCM, furnishing the dinitrogen complexes $[Cp^*Ru(N_2)(\kappa^2\text{-}P,N\text{-}^iPr_2PCH_2X)][BAr'_4]$ [X = Py (**8a**), Quin (**8b**)]. These compounds display strong $\nu(N_2)$ bands in their IR spectra at 2169 cm^{-1} for **8a** and at 2152 cm^{-1} for **8b**. These values indicate little degree of back-donation from the metal to the coordinated dinitrogen and, hence, little activation of the N≡N bond, as has been typically observed in other half-sandwich Ru−N_2 complexes.[46,51,52] Exposure of **5b** or **8b** to air in CD_2Cl_2 led to the formation of the dioxygen complex

(50) (a) Baya, M.; Maresca, O.; Poli, R.; Coppel, Y.; Maseras, F.; Lledós, A.; Belkova, N. V.; Dub, P. A.; Epstein, L. M.; Shubina, E. S. *Inorg. Chem.* **2006**, *45*, 10248–10262. (b) Rossin, A.; Gonsalvi, L.; Phillips, A. D.; Maresca, O.; Lledos, A.; Peruzzini, M. *Organometallics* **2007**, *26*, 3289–3296.

(51) Aneetha, H.; Jiménez-Tenorio, M.; Puerta, M. C.; Valerga, P.; Mereiter, K. *Organometallics* **2002**, *21*, 628–635.

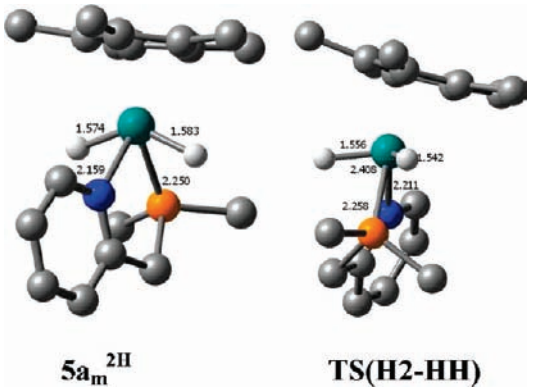

Figure 18. Optimized geometries of the *trans*-dihydride complex $\mathbf{5a_m^{2H}}$ and the transition state for the dihydrogen−dihydride interconversion [**TS(H2-HH)**].

[Cp*Ru(O_2)(κ^2-P,N-^{i}Pr$_2$PCH$_2$Quin)][BAr′$_4$] (**9b**). However, exposure of **5a** or **8a** to air led to the formation of a mixture of uncharacterized species, which at this stage were not further investigated. The X-ray crystal structures of **8b** and **9b** were determined. ORTEP views of the complex cations [Cp*Ru(N_2)(κ^2-P,N-^{i}Pr$_2$PCH$_2$Quin)]$^+$ in **8b** and [Cp*Ru(O_2)(κ^2-P,N-^{i}Pr$_2$PCH$_2$Quin)]$^+$ in **9b** are shown in Figures 19 and 20, respectively, together with the most relevant bond distances and angles.

The complex cation in **8b** shows a "three-legged-piano-stool" structure, with the dinitrogen ligand bound in an end-on manner. The Ru−N1−N2 angle of 172.06(19)° indicates an almost linear Ru−N_2 assembly, with a Ru−N1 separation of 1.9925(19) Å and a N1−N2 bond length of 1.096(3) Å. These bond distances compare well with those reported for other half-sandwich Ru−N_2 complexes such as [CpRu(N_2)(dippe)][BAr′$_4$] [Ru−N1 1.961(3) Å; N1−N2 1.087(4) Å][51] or [Cp*Ru(N_2)(dppm)][BAr′$_4$] [Ru−N1 1.975(2) Å; N1−N2 1.083(4) Å].[52] As is usual in terminal dinitrogen complexes, the N−N separation in **8b** is essentially identical with that corresponding to the free dinitrogen molecule. The complex cation **9b** also displays a "three-legged-piano-stool" structure, with the dioxygen ligand bound in a side-on manner, having an O1−O2 separation of 1.398(4) Å, which is very similar to that found in [Cp*Ru(O_2)(L-L′)][BPh$_4$] [1.394(9) Å; L-L′ = 1,3-(dioxan-2-ylmethyl)diphenylphosphine],[53] and also in [Cp*Ru(O_2)-(dppe)][PF$_6$] [1.398(5) Å].[54] These distances are intermediate between those in the free dioxygen molecule and in the ionic peroxide anion (1.49 Å). The Ru−O bond lengths of 2.011(3) and 2.040(3) Å suggest an essentially symmetrical arrangement of the dioxygen ligand, very similar to that found in related complexes.

The dihydrogen complexes **5a** and **5b** release dihydrogen when they are dissolved in CD_2Cl_2 under argon, leading to bluish to greenish solutions. This tendency is even greater for compound **5a**, which loses dihydrogen in the solid state under argon. This process involves a color change from yellow to greenish blue. The blue color is attributed to the formation of the coordinatively unsaturated 16-electron species [Cp*Ru(κ^2-P,N-^{i}Pr$_2$PCH$_2$Py)]$^+$ and [Cp*Ru(κ^2-P,N-^{i}Pr$_2$PCH$_2$Quin)]$^+$. These extremely air-sensitive species are homologues of the 16-electron cationic complexes [Cp*Ru(PP)]$^+$ [PP = dippe, (PMe^{i}Pr$_2$)$_2$, (PEt$_3$)$_2$][42] and [Cp*Ru(NN)]$^+$ [NN = Me$_2$NCH$_2$CH$_2$NR$_2$, where R$_2$ = Me$_2$, ^{t}Bu$_2$, (CH$_2$CH$_2$)$_2$O].[55,56] We have been able to isolate the blue complex [Cp*Ru(κ^2-P,N-^{i}Pr$_2$-PCH$_2$Py)][BAr′$_4$] (**10a**) either by the reaction of **1a** with NaBAr′$_4$ in fluorobenzene under argon or by pumping in vacuo crystals of the dihydrogen complex **5a** (Chart 7).

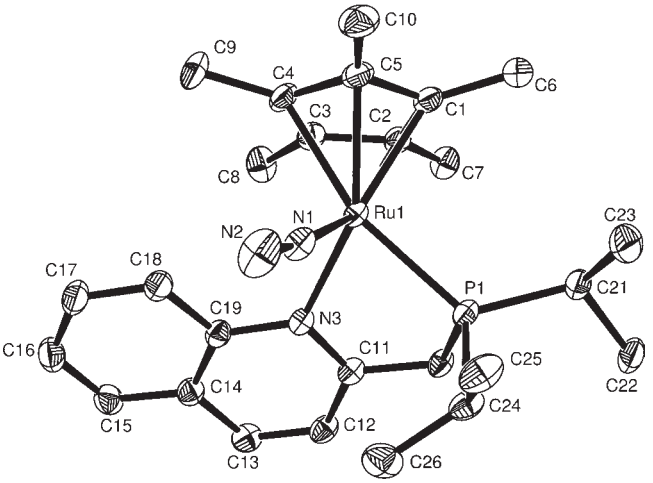

Figure 19. ORTEP drawing (50% thermal ellipsoids) of the cation [Cp*Ru(N_2)(κ^2-P,N-^{i}Pr$_2$PCH$_2$Quin)]$^+$ in complex **8b**. Hydrogen atoms have been omitted. Selected bond lengths (Å) and angles (deg) with estimated standard deviations in parentheses: Ru1−P1 2.3335(7), Ru1−N1 1.9925(19), Ru1−N3 2.1730(19), Ru1−C1 2.209(2), Ru1−C2 2.177(2), Ru1−C3 2.219(2), Ru1−C4 2.238(2), Ru1−C5 2.204(2), N1−N2 1.096(3); P1−Ru1−N1 95.35(5), P1−Ru1−N3 78.87(4), N1−Ru1−N3 91.86(8), Ru1−N1−N2 172.06(19).

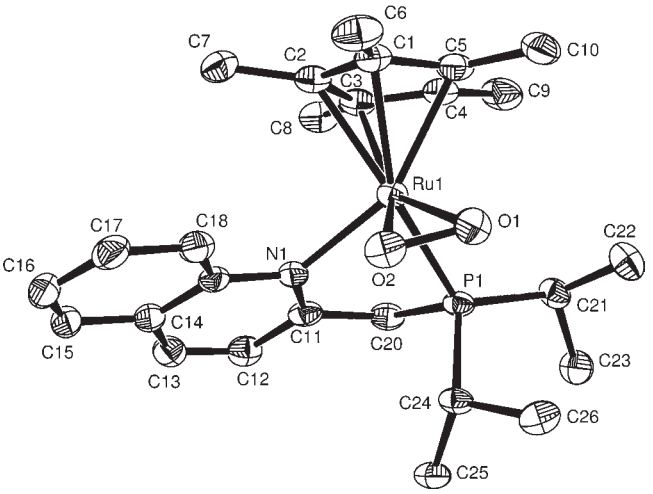

Figure 20. ORTEP drawing (50% thermal ellipsoids) of the cation [Cp*Ru(O_2)(κ^2-P,N-^{i}Pr$_2$PCH$_2$Quin)]$^+$ in **9b**. Hydrogen atoms have been omitted. Selected bond lengths (Å) and angles (deg) with estimated standard deviations in parentheses: Ru1−P1 2 2.3079(10), Ru1−N1 2.165(3), Ru1−O1 2.011(3), Ru1−O2 2.040(3), Ru1−C1 2.259(4), Ru1−C2 2.256(4), Ru1−C3 2.205(4), Ru1−C4 2.264(4), Ru1−C5 2.245(4), O1−O2 1.398(4); P1−Ru1−N1 76.31(9), O1−Ru1−O2 40.36(11).

(52) Aneetha, H.; Jiménez-Tenorio, M.; Puerta, M. C.; Valerga, P.; Mereiter, K. *Organometallics* **2003**, *22*, 1779–1782.
(53) Lindner, E.; Haustein, M.; Fawzi, R.; Steinmann, M.; Wegner, P. *Organometallics* **1994**, *13*, 5021–5029.
(54) Kirchner, K.; Mauthner, K.; Mereiter, K.; Schmidt, R. *J. Chem. Soc., Chem. Commun*. **1993**, 892–893.
(55) Gemel, C.; Mereiter, K.; Schmid, R.; Kirchner, K. *Organometallics* **1997**, *16*, 5601–5603.
(56) Gemel, C.; Sapunov, V. N.; Mereiter, K.; Ferencic, M.; Schmid, R.; Kirchner, K. *Inorg. Chim. Acta* **1999**, *286*, 114–120.

Chart 7

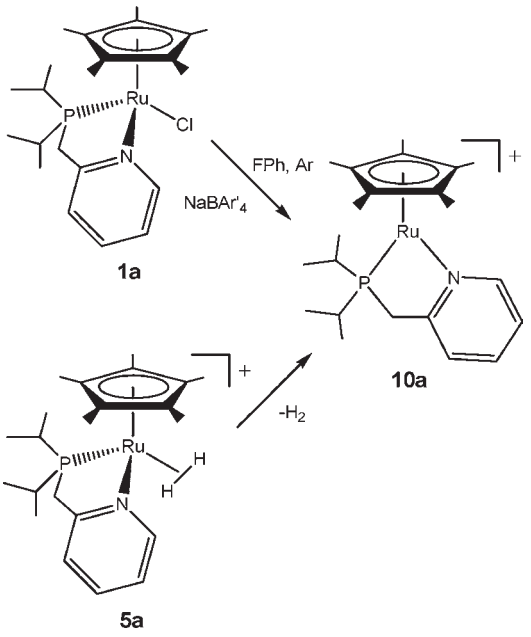

The 16-electron complex **10a** is exceedingly reactive. It turns brown in the solid state when stored for a few days. It also decomposes in solution in most organic solvents. It was characterized by NMR spectroscopy in fluorobenzene-d_5, where it appears to be more stable. The NMR spectra at 298 K consist of broad features, which become sharper at low temperatures. The ^{1}H NMR spectrum at 238 K is consistent with the presence of a κ^2-P,N-^{i}Pr$_2$PCH$_2$Py ligand. The hydrogen atoms of the CH_2 spacer group are inequivalent and appear shifted to an unusually high field, i.e., from 2.87 ppm (H_a in **5a**) to 1.00 (H_a in **10a**). The H_a-H_b correlations as well as the CH_a-H_b correlations were confirmed by means of g-COSY and g-HSQC NMR spectra, respectively. If we assume a "two-legged-piano-stool" structure for **10a**, analogous to that found for other 16-electron Cp*Ru(PP)$^+$ and Cp*Ru(NN)$^+$ complexes,[42,55,56] we find that the five-membered ring RuNCCP is relatively rigid but not planar. Hence, the hydrogen atoms of the PCH_2 group can still adopt two inequivalent, mutually exchangeable positions through a hindered rotation around the $P-CH_2$ bond, as shown in Chart 8.

Alternatively, we might consider that the structure of **10a** is bent or pyramidalized.[56−58] DFT studies have shown that variation of the ground-state energy of the model compound [CpRu($PH_2CH_2CH_2PH_2$)]$^+$ reaches a minimum with a value for the pyramidalization angle α between 149° and 152°, whereas in the case of [CpRu($NH_2CH_2CH_2NH_2$)]$^+$, the minimum is reached for α between 171° and 179° (structure not pyramidalized).[57,58] A pyramidalized structure should involve the dynamic exchange between two possible configurations, in which the atoms H_a and H_b interconvert each other as a result (Chart 9).

(57) Brunner, H.; Tsuno, T. *Acc. Chem. Res.* **2009**, *42*, 1501–1510.
(58) The pyramidalization angle α is defined as the angle formed by the centroid of the Cp* ring, the ruthenium atom, and the centroid of the moiety L−Ru−L (L = P, N).

Chart 8

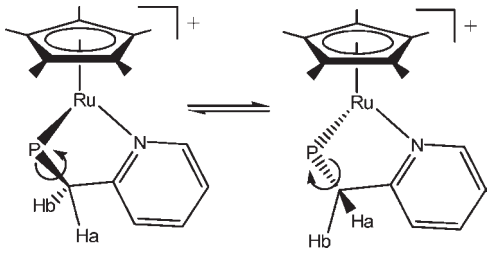

Chart 9

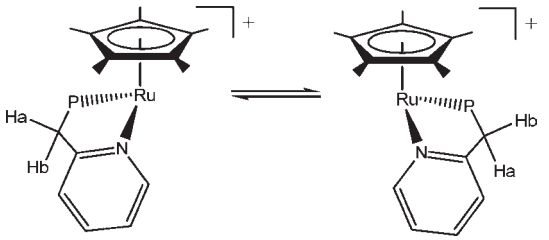

It is important to mention that the C5-ring resonance for **10a** appears in the ^{13}C{^{1}H} NMR spectrum as a broad signal at 80.2 ppm. The position of the C5-ring resonance allows one to distinguish between half-sandwich 16- and 18-electron complexes. This resonance appears in the range 70−81 ppm in the case of 16-electron complexes and between 81 and 100 ppm in the case of 18-electron complexes.[42] Hence, this spectral feature for **10a** is fully consistent with its formulation as a coordinatively unsaturated species.

To structurally characterize the 16-electron compounds, we have optimized the real complex **10b** and the model complex $\mathbf{10a_m}$. Their structures are depicted in Figure 17. Both exhibit a pyramidalized geometry, with values of the pyramidalization angle α of 153.8° and 160.8° for **10b** and $\mathbf{5a_m}$, respectively. These values can be compared with those of the corresponding 18-electron dihydrogen complexes **5b** and $\mathbf{5a_m}$ (140.2° and 146.0°, respectively). We have checked for the small complex $\mathbf{10a_m}$ the relative energy of the triplet state. The optimized triplet is found 51.8 kJ mol^{-1} above the singlet, pointing out the low-spin character of the ground state for this unsaturated complex.

Conclusions

The proton-transfer reactions to the trihydride complexes **2a** and **2b** using both weak and strong acids have been experimentally studied and theoretically modeled by DFT calculations. The reactions with weak donors result in the formation of hydrogen-bonded adducts between the proton donor and the pendant pyridine or quinoline group. This has been unequivocally demonstrated by determination of the X-ray crystal structure of the supramolecular aggregate **3a**. Proton transfer to the hydride ligands can be modulated by solvent polarity. Protonation with CF_3SO_3H in CD_2Cl_2 occurs in a stepwise manner involving protonation at the pendant nitrogen atom followed by hydrogen transfer to the hydride, dihydrogen elimination, and formation of the dihydrogen complexes **5a**/**5b**, which do not rearrange to their dihydride isomers. With an excess of acid, a second protonation occurs at the hydride site and the dicationic complexes

6a or **6b** are generated. Dihydrogen elimination from **5a**/**5b** generates highly reactive 16-electron complexes that exhibit bent or pyramidalized structures, as inferred from spectral and DFT calculations. These unsaturated complexes provide binding sites for other small molecules such as dinitrogen or dioxygen. The ability of the pendant pyridyl or quinoline groups to interact with weak proton donors suggests the possibility of using the hydride complexes **2a**/**2b** as catalyst precursors for a number of transformations in polar media such as nitrile hydration reactions. These studies are currently being carried out and will be reported in due course.

Experimental Section

All synthetic operations were performed under a dry dinitrogen or argon atmosphere following conventional Schlenk techniques. Tetrahydrofuran, diethyl ether, and petroleum ether (boiling point range 40−60 °C) were obtained oxygen- and water-free from an Innovative Technology, Inc., solvent purification apparatus. Toluene and other solvents were of anhydrous quality and were used as received. All solvents were deoxygenated immediately before use. The ligands $^{i}Pr_2PCH_2Py$ and $^{i}Pr_2PCH_2Quin$ were respectively prepared by the reaction of $LiCH_2Py$ and $LiCH_2Quin$ with $^{i}Pr_2PCl$, following suitable adaptations of published procedures.[59] $[\{Cp^*RuCl\}_4]$[60] and $NaBAr'_4$[61] were prepared according to literature methods. CF_3SO_3H, indole, benzoic acid, and salicylic acid were used as supplied by Aldrich. IR spectra were taken in Nujol mulls on a Perkin-Elmer Spectrum 1000 FTIR spectrophotometer. NMR spectra were taken on Varian Unity 400 MHz or Varian Inova 600 MHz equipment. Chemical shifts are given in ppm from $SiMe_4$ (^1H and $^{13}C\{^1H\}$), 85% H_3PO_4 ($^{31}P\{^1H\}$), or $CFCl_3$ (^{19}F). Longitudinal relaxation time (T_1) measurements were made by the inversion−recovery method. Activation parameters for fluxional processes were obtained by a dynamic NMR line-shape fitting simulation using the program *DNMR3*[62] incorporated into *SpinWorks 2.4*.[63] Microanalysis was performed on elemental analyzer model LECO CHNS-932 at the Servicio Central de Ciencia y Tecnología, Universidad de Cádiz.

$[Cp^*RuCl(\kappa^2\text{-}P,N\text{-}^{i}Pr_2PCH_2Py)]$ (1a) and $[Cp^*RuCl(\kappa^2\text{-}P,N\text{-}^{i}Pr_2PCH_2Quin)]$ (1b). To $[\{Cp^*RuCl\}_4]$ (0.66 g, ca. 0.6 mmol) in petroleum ether (20 mL) was added via syringe either $^{i}Pr_2PCH_2Py$ (0.65 mL, ca. 2.5 mmol) or $^{i}Pr_2PCH_2Quin$ (0.75 mL, ca. 2.5 mmol). The resulting red (for **1a**) or black (for **1b**) suspension was stirred at room temperature for 30 min. Then, the microcrystalline precipitate was filtered off, washed with petroleum ether, and dried in vacuo. The resulting products were pure enough for synthetic purposes. Both **1a** and **1b** could be recrystallized from hot toluene/petroleum ether in the form of red-orange or black crystals. Yield: 90% in both cases (65−70% upon recrystallization). Data for **1a**. Anal. Calcd for $C_{22}H_{35}NClPRu$: C, 54.9; H, 7.33; N, 2.9. Found: C, 54.8; H, 7.01; N, 2.6. ^1H NMR (400 MHz, C_6D_6, 298 K): δ 0.67 (m, 3 H), 0.99 (m, 3 H), 1.27 (m, 6 H) $[P(CH(CH_3)_2)_2]$, 1.66 [s, 15 H, $C_5(CH_3)_5$], 2.07, 2.49 [m, 1 H each, $P(CH(CH_3)_2)_2$], 2.63 (dd, $^2J_{HH}$ = 15.6 Hz, $^2J_{HP}$ = 9.7 Hz, 1 H, PCH_aH_b), 3.47 (dd, $^2J_{HH}$ = 15.6 Hz, $^2J_{HP}$ = 8.2 Hz, 1 H, PCH_aH_b), 6.39 (t), 6.61 (d), 6.80 (t), 8.87 (d) (1 H each, C_5H_4N). $^{31}P\{^1H\}$ NMR (161.89 MHz, C_6D_6, 298 K): δ 75.5 (s). $^{13}C\{^1H\}$ NMR (101 MHz, C_6D_6, 298 K): δ 10.95 [s, $C_5(CH_3)_5$], 17.83, 18.84, 19.57 [s, $P(CH(CH_3)_2)_2$], 25.30 [d, $^1J_{CP}$ = 16.3 Hz, $PCH(CH_3)_2$], 25.82 [d, $^1J_{CP}$ = 17.9 Hz, $PCH(CH_3)_2$], 35.99 (d, $^1J_{CP}$ = 16.3 Hz, PCH_2), 82.18 [s, $C_5(CH_3)_5$], 121.17, 121.57, 134.00, 154.78, 164.20 (C_5H_4N). Data for **1b**. Anal. Calcd for $C_{26}H_{37}NClPRu$: C, 58.8; H, 7.02; N, 2.6. Found: C, 58.8; H, 6.91; N, 2.5. ^1H NMR (400 MHz, CD_2Cl_2, 298 K): δ 0.74 (m, 3 H), 1.10 (m, 3 H), 1.48 (m, 3 H), 1.58 (m, 3H) $[P(CH(CH_3)_2)_2]$, 1.37 [s, 15 H, $C_5(CH_3)_5$], 2.21, 2.63 [m, 1 H each, $P(CH(CH_3)_2)_2$], 3.16 (dd, $^2J_{HH}$ = 16.4 Hz, $^2J_{HP}$ = 3.5 Hz, 1 H, PCH_aH_b), 3.57 (dd, $^2J_{HH}$ = 16.4 Hz, $^2J_{HP}$ = 10 Hz, 1 H, PCH_aH_b), 7.40 (d), 7.49 (t), 7.71 (m), 7.73 (m), 7.90 (d), 9.67 (d) (C_9H_6N). $^{31}P\{^1H\}$ NMR (161.89 MHz, CD_2Cl_2, 298 K): δ 51.7 (s). $^{13}C\{^1H\}$ NMR (101 MHz, CD_2Cl_2, 298 K): δ 10.31 [s, $C_5(CH_3)_5$], 18.86, 19.97, 20.13, 21.09 [s, $P(CH(CH_3)_2)_2$], 26.33 [d, $^1J_{CP}$ = 10.1 Hz, $PCH(CH_3)_2$], 28.36 [d, $^1J_{CP}$ = 20.1 Hz, $PCH(CH_3)_2$], 43.60 (d, $^1J_{CP}$ = 18.9 Hz, PCH_2), 81.11 [s, $C_5(CH_3)_5$], 119.39, 126.67, 127.23, 128.42, 128.99, 134.82, 134.87, 151.46, 163.22 (C_9H_6N).

$[Cp^*RuH_3(\kappa^1\text{-}P\text{-}^{i}Pr_2PCH_2Py)]$ (2a) and $[Cp^*RuH_3(\kappa^1\text{-}P\text{-}^{i}Pr_2PCH_2Quin)]$ (2b). To **1a** or **1b** (1 mmol) in MeOH (15 mL) at 0 °C (ice bath) was carefully added in small portions an excess of solid $NaBH_4$ (0.3 g). ***Caution!*** *Strong dihydrogen evolution will occur*. Once the addition was finished, the ice bath was removed and the mixture stirred for 10−15 min at room temperature. Then, the solvent was removed in vacuo. The residue was extracted with two portions of 10 mL of petroleum ether and filtered through an anhydrous Na_2SO_4 plug. The resulting solution was concentrated to ca. 3 mL and cooled to −20 °C. Colorless crystals were obtained that were filtered off and dried in vacuo. **2a** and **2b** can also be obtained directly from $[\{Cp^*RuCl_2\}_n]$ by reaction with the appropriate amount of the corresponding phosphine $^{i}Pr_2PCH_2Py$ or $^{i}Pr_2PCH_2Quin$ and an excess of solid $NaBH_4$ in MeOH at 0 °C. Data for **2a**. Yield: 0.27 g, 60%. Anal. Calcd for $C_{22}H_{38}NPRu$: C, 58.9; H, 8.54; N, 3.1. Found: C, 58.7; H, 8.61; N, 2.9. IR: ν(Ru−H) 1986 cm^{-1}. ^1H NMR (400 MHz, toluene-d_8, 298 K): δ −10.92 (d, $^2J_{HP}$ = 21.8 Hz, 3 H, RuH_3), 0.99 [m, 12 H, $P(CH(CH_3)_2)_2$], 1.87 [m, 2 H, $P(CH(CH_3)_2)_2$], 2.00 [s, 15 H, $C_5(CH_3)_5$], 3.06 (d, $^2J_{HP}$ = 9.2 Hz, PCH_2), 6.60 (t), 7.00 (t), 7.03 (d), 8.33 (d) (1 H each, C_5H_4N ring). $^{31}P\{^1H\}$ NMR (161.89 MHz, toluene-d_8, 298 K): δ 88.7 (s). $^{13}C\{^1H\}$ NMR (101 MHz, toluene-d_8, 298 K): δ 12.61 $[C_5(CH_3)_5]$, 18.80, 19.38 $[P(CH(CH_3)_2)_2]$, 27.80 [d, $^1J_{PC}$ = 26 Hz, $P(CH(CH_3)_2)_2$], 42.55 (d, $^1J_{PC}$ = 17.9 Hz, PCH_2), 94.94 [$C_5(CH_3)_5$], 120.72, 135.24, 137.47, 149.19, 159.06 (C_5H_4N ring). Data for **2b**. Yield: 0.33 g, 66%. Anal. Calcd for $C_{26}H_{40}NPRu$: C, 62.6; H, 8.09; N, 2.8. Found: C, 62.7; H, 8.18; N, 2.6. IR: ν(Ru−H) 1989 cm^{-1}. ^1H NMR (400 MHz, toluene-d_8, 298 K): δ −10.82 (d, $^2J_{HP}$ = 22 Hz, 3 H, RuH_3), 1.05 [m, 12 H, $P(CH(CH_3)_2)_2$], 1.90 [m, 2 H, $P(CH(CH_3)_2)_2$], 2.02 [s, 15 H, $C_5(CH_3)_5$], 3.25 (d, $^2J_{HP}$ = 9.2 Hz, PCH_2), 7.13, 7.23, 7.34, 7.36, 7.51, 8.05 (m, 1 H each, C_9H_6N ring). $^{31}P\{^1H\}$ NMR (161.89 MHz, toluene-d_8, 298 K): δ 89.1 (s). $^{13}C\{^1H\}$ NMR (101 MHz, toluene-d_8, 298 K): δ 12.95 $[C_5(CH_3)_5]$, 19.21, 19.68 $[P(CH(CH_3)_2)_2]$, 28.52 [d, $^1J_{PC}$ = 25 Hz, $P(CH(CH_3)_2)_2$], 43.56 (d, $^1J_{PC}$ = 16.9 Hz, PCH_2), 95.34 $[C_5(CH_3)_5]$, 124.31, 126.00, 127.25, 128.02, 129.50, 129.94, 135.31, 148.91, 159.80 (C_9H_6N ring).

$[Cp^*RuH_3(\kappa^1\text{-}P\text{-}^{i}Pr_2PCH_2Py)]\cdot C_6H_4(OH)COOH$ (3a). To a solution of **2a** (0.23 g, ca. 0.5 mmol) in toluene was added salicylic acid (0.07 g, ca. 0.5 mmol). The mixture was stirred at room temperature for 2 h. Then, the solvent was removed in vacuo and the orange residue washed with petroleum ether. The product was dissolved in a minimum amount of toluene and the solution filtered. The solution was layered with petroleum ether. Slow diffusion of petroleum ether into the concentrated toluene solution afforded well-formed orange crystals, suitable for X-ray structure analysis. Yield: 0.16 g, 55%. Anal. Calcd for $C_{29}H_{44}NO_3PRu$: C, 59.4; H, 7.56; N, 2.4. Found: C, 59.4; H, 7.48; N, 2.2. IR: ν(Ru−H) 1979 cm^{-1}, ν(C=O) 1596 cm^{-1}. ^1H NMR (400 MHz, C_6D_6, 298 K): δ −10.84 (d, $^2J_{HP}$ = 21.5 Hz,

(59) Jansen, A.; Pitter, S. *Monatsch. Chem.* **1999**, *130*, 783–794.
(60) (a) Fagan, P. J.; Ward, M. D.; Calabrese, J. C. *J. Am. Chem. Soc.* **1989**, *111*, 1698–1719. (b) Fagan, P. J.; Mahoney, W. S.; Calabrese, J. C.; Williams, I. D. *Organometallics* **1990**, *9*, 1843–1852.
(61) Brookhart, M.; Grant, B.; Volpe, A. F. *Organometallics* **1992**, *11*, 3920–3922.
(62) Kleier, D. A.; Binsch, G. *J. Magn. Reson.* **1970**, *3*, 146–160.
(63) Marat, K. *SpinWorks 2.4*; University of Manitoba: Winnipeg, Manitoba, Canada, **2005**.

3 H, RuH_3), 0.97 [m, 12 H, P(CH(CH_3)$_2$)$_2$], 1.90 [m, 2 H, P(CH(CH$_3$)$_2$)$_2$], 1.98 [s, 15 H, C$_5$(CH_3)$_5$], 3.12 (d, $^2J_{HP}$ = 9.3 Hz, PCH_2), 6.53 (m), 6.95 (td), 7.21 (d), 8.42 (d) (1 H each, C$_5H_4$N ring protons), 6.70 (t br), 7.05 (d), 7.11 (m), 8.21 (d br) (1 H each, C$_6H_4$ ring protons), 10.5 (br, 2 H, COOH + OH). ^{31}P{^{1}H} NMR (161.89 MHz, C$_6$D$_6$, 298 K): δ 90.7 (s br). ^{13}C{^{1}H} NMR (101 MHz, C$_6$D$_6$, 298 K): δ 12.50 [C$_5$(CH_3)$_5$], 18.58, 19.22 [P(CH(CH_3)$_2$)$_2$], 27.81 [d, $^1J_{PC}$ = 24.3 Hz, P(CH(CH$_3$)$_2$)$_2$], 40.87 (d, $^1J_{PC}$ = 17 Hz, PCH_2), 95.08 [C$_5$(CH$_3$)$_5$], 117.74, 118.75, 131.0, 135.12, 163.23 (C$_6$H$_4$ ring), 121.31, 125.86, 136.54, 147.56, 157.90 (C$_5$H$_4$N ring), 174.11 (COOH). ^{1}H NMR (400 MHz, CD$_2$Cl$_2$, 298 K): δ −11.32 (br, RuH_3), 0.93 [m, 12 H, P(CH-(CH_3)$_2$)$_2$], 1.90 [m, 2 H, P(CH(CH$_3$)$_2$)$_2$], 2.00 [s, 15 H, C$_5$(CH_3)$_5$], 3.16 (d, $^2J_{HP}$ = 9.2 Hz, PCH_2), 6.83 (t), 6.88 (d), 7.37 (t), 7.88 (d br) (1 H each, C$_6H_4$ ring protons), 7.26 (m), 7.49 (d), 7.73 (t), 8.59 (d) (1 H each, C$_5H_4$N ring protons), 9.90 (br, COOH + OH). ^{31}P{^{1}H} NMR (161.89 MHz, CD$_2$Cl$_2$, 298 K): δ 91.1 (s br). ^{13}C{^{1}H} NMR (101 MHz, CD$_2$Cl$_2$, 298 K): δ 12.40 [C$_5$(CH_3)$_5$], 18.50, 19.18 [P(CH(CH_3)$_2$)$_2$], 27.76 [d, $^1J_{PC}$ = 25.1 Hz, P(CH-(CH$_3$)$_2$)$_2$], 40.35 (d, $^1J_{PC}$ = 17.9 Hz, PCH_2), 95.35 [C$_5$(CH$_3$)$_5$], 117.023, 118.52, 130.95, 134.32, 162.24 (C$_6$H$_4$ ring), 121.97, 126.32, 137.67, 147.07, 157.73 (C$_5$H$_4$N ring).

[Cp*Ru(H$_2$)(κ^2-P,N-^{i}Pr$_2$PCH$_2$Py)][BAr′$_4$] (5a) and [Cp*Ru(H$_2$)-(κ^2-P,N-^{i}Pr$_2$PCH$_2$Quin)][BAr′$_4$] (5b). To an equimolar mixture of **1a** or **1b** and NaBAr′$_4$ (0.5 mmol) under dihydrogen was added diethyl ether (20 mL). The mixture was stirred under dihydrogen for 1 h. Then it was filtered through an anhydrous Na$_2$SO$_4$ plug. The solution was layered with petroleum ether in a countercurrent of dihydrogen and left to stand at room temperature in a dihydrogen atmosphere. Yellow crystals were obtained that were filtered off and dried in an argon stream. They were stored under dihydrogen. Otherwise, they lose dihydrogen gradually, much quicker in the case of **5a**. NMR were recorded under dihydrogen. Data for **5a**. Yield: 0.39 g, 60%. Anal. Calcd for C$_{54}$H$_{49}$NBF$_{24}$PRu: C, 49.5; H, 3.77; N, 1.1. Found: C, 49.6; H, 3.61; N, 1.0. ^{1}H NMR (400 MHz, CD$_2$Cl$_2$, 298 K): δ −6.63 [br, 2 H, $(T_1)_{min}$ = 10 ms, Ru(H_2)], 0.73 (m, 3 H), 0.88 (m, 3 H), 1.12 (m, 3 H), 1.24 (m, 3 H) [P(CH(CH_3)$_2$)$_2$], 1.76 [s, 15 H, C$_5$(CH_3)$_5$], 2.27, 2.46 [m, 1 H each, P(CH(CH$_3$)$_2$)$_2$], 2.87 (dd, 1 H, $^2J_{HP}$ = 7.74 Hz, $^2J_{HaHb}$ = 17.4 Hz, PCH_aH$_b$), 3.32 (dd, 1 H, $^2J_{HP}$ = 10.5 Hz, $^2J_{HaHb}$ = 17.4 Hz, PCH$_a$$H_b$), 7.17 (t), 7.38 (d), 7.63 (t), 8.60 (d) (1 H each, C$_5H_4$N). ^{31}P{^{1}H} NMR (161.89 MHz, CD$_2$Cl$_2$, 298 K): δ 84.5 (s). ^{13}C{^{1}H} NMR (101 MHz, CD$_2$Cl$_2$, 298 K): δ 10.92 [s, C$_5$(CH_3)$_5$], 18.34 [br, P(CH-(CH_3)$_2$)$_2$], 24.37 [br, PCH(CH$_3$)$_2$], 36.90 (d, $^1J_{CP}$ = 23.5 Hz, PCH_2), 92.9 [s, C$_5$(CH$_3$)$_5$], 123.77, 138.43, 156.20, 163.22 (C$_5$H$_4$N). Data for **5b**. Yield: 0.47 g, 69%. Anal. Calcd for C$_{58}$H$_{51}$NBF$_{24}$PRu: C, 51.2; H, 3.78; N, 1.0. Found: C, 51.2; H, 3.60; N, 0.9. ^{1}H NMR (400 MHz, CD$_2$Cl$_2$, 298 K): δ −5.62 [br, 2 H, $(T_1)_{min}$ = 11 ms, Ru(H_2)], 0.18 (m, 3 H), 0.94 (m, 3 H), 1.46 (m, 6 H) [P(CH(CH_3)$_2$)$_2$], 1.58 [s, 15 H, C$_5$(CH_3)$_5$], 2.06, 2.69 [m, 1 H each, P(CH(CH$_3$)$_2$)$_2$], 3.74 (dd, 1 H, $^2J_{HP}$ = 5.5 Hz, $^2J_{HaHb}$ = 17.6 Hz, PCH_aH$_b$), 3.91 (dd, 1 H, $^2J_{HP}$ = 12.6 Hz, $^2J_{HaHb}$ = 17.6 Hz, PCH$_a$$H_b$), 7.70 (m, 2 H), 7.92 (m, 2 H), 8.27 (d, 1 H), 8.94 (d, 1 H) (C$_9H_6$N). ^{31}P{^{1}H} NMR (161.89 MHz, CD$_2$Cl$_2$, 298 K): δ 77.8 (s). ^{13}C(^{1}H) NMR (158.83 MHz, CD$_2$Cl$_2$, 253 K): δ 10.48 [s, C$_5$(CH_3)$_5$], 17.71, 18.01, 18.24, 18.78 [s, P(CH(CH_3)$_2$)$_2$], 22.20 [d, $^1J_{CP}$ = 23 Hz, PCH(CH$_3$)$_2$], 27.50 [d, $^1J_{CP}$ = 23.2 Hz, PCH(CH$_3$)$_2$], 43.72 (d, $^1J_{CP}$ = 23 Hz, PCH_2), 92.56 [s, C$_5$-(CH$_3$)$_5$], 120.68, 127.54, 128.94, 131.16, 132.19, 139.38, 148.95, 165.91 (C$_9$H$_6$N).

[Cp*Ru(N$_2$)(κ^2-P,N-^{i}Pr$_2$PCH$_2$Py)][BAr′$_4$] (8a) and [Cp*Ru-(N$_2$)(κ^2-P,N-^{i}Pr$_2$PCH$_2$Quin)][BAr′$_4$] (8b). To an equimolar mixture of **1a** or **1b** and NaBAr′$_4$ (0.5 mmol) under dinitrogen was added diethyl ether (20 mL). The mixture was stirred under dinitrogen for 1 h. Then it was filtered through an anhydrous Na$_2$SO$_4$ plug. The solution was concentrated by passing through a dinitrogen stream. Layering the solution with petroleum ether afforded red-orange crystals, which were filtered off and dried in a dinitrogen stream. Data for **8a**. Yield: 0.43 g, 64%. Calcd for C$_{54}$H$_{47}$N$_3$BF$_{24}$PRu: C, 48.5; H, 3.54; N, 3.1. Found: C, 48.3; H, 3.61; N, 2.9. IR: ν(N$_2$) 2169 cm^{-1}. ^{1}H NMR (400 MHz, tetrahydrofuran-d_8, 298 K): δ 0.97 (m br, 6 H), 1.23 [m br, 6 H, P(CH(CH_3)$_2$)$_2$], 1.62 [s, 15 H, C$_5$(CH_3)$_5$], 2.45, 2.97 [m br, 1 H each, P(CH(CH$_3$)$_2$)$_2$], 3.32, 3.58 (br, 1 H each, PCH_2), 7.27 (t), 7.39 (d), 7.72 (t), 9.09 (d) (1 H each, C$_5H_4$N). ^{31}P{^{1}H} NMR (161.89 MHz, tetrahydrofuran-d_8, 298 K): δ 75.4 (s). ^{13}C{^{1}H} NMR (101 MHz, tetrahydrofuran-d_8, 323 K): δ 10.67 [s, C$_5$(CH_3)$_5$], 18.21, 19.29 [s, P(CH(CH_3)$_2$)$_2$], 25.49 [s br, PCH(CH$_3$)$_2$], 33.97 (s br, PCH_2), 82.42 [s, C$_5$(CH$_3$)$_5$], 123.61, 137.73, 165.39 (C$_5$H$_4$N). Data for **8b**. Yield: 0.53 g, 76%. Calcd for C$_{58}$H$_{49}$N$_3$BF$_{24}$PRu: C, 50.2; H, 3.56; N, 3.0. Found: C, 50.0; H, 3.48; N, 2.9. IR: ν(N$_2$) 2152 cm^{-1}. ^{1}H NMR (400 MHz, CD$_3$NO$_2$, 298 K): δ 0.72 (m, 3 H), 1.02 (m, 3 H), 1.55 (m, 3 H), 1.60 (m, 3H) [P(CH(CH_3)$_2$)$_2$], 1.41 [s, 15 H, C$_5$(CH_3)$_5$], 2.68, 2.80 [m, 1 H each, P(CH(CH$_3$)$_2$)$_2$], 3.84 (dd, $^2J_{HH}$ = 18.4 Hz, $^2J_{HP}$ = 5.9 Hz, 1 H, PCH_aH$_b$), 4.15 (dd, $^2J_{HH}$ = 18.4 Hz, $^2J_{HP}$ = 13.9 Hz, 1 H, PCH$_a$$H_b$), 7.81 (m), 7.83 (t), 8.06 (d), 8.08 (m), 8.54 (d), 8.69 (d) (C$_9H_6$N). ^{31}P{^{1}H} NMR (161.89 MHz, CD$_3$NO$_2$, 298 K): δ 77.4 (s). ^{13}C{^{1}H} NMR (101 MHz, CD$_2$Cl$_2$, 298 K): δ 9.55 (s, C$_5$(CH_3)$_5$), 18.56, 18.89, 18.89, 20.10 [s, P(CH(CH_3)$_2$)$_2$], 26.00 [d, $^1J_{CP}$ = 21.1 Hz, PCH(CH$_3$)$_2$], 29.25 [d, $^1J_{CP}$ = 26 Hz, PCH(CH$_3$)$_2$], 40.00 (d, $^1J_{CP}$ = 27.7 Hz, PCH_2), 95.34 [s, C$_5$-(CH$_3$)$_5$], 108.60, 122.63, 129.66, 134.09, 136.92, 143.64 (C$_9$H$_6$N).

[Cp*Ru(O$_2$)(κ^2-P,N-^{i}Pr$_2$PCH$_2$Quin)][BAr′$_4$] (9b). This compound was obtained following an experimental procedure identical with that for **8a**/**8b** but using air instead of dinitrogen. Alternatively, it can be prepared quantitatively by stirring a diethyl ether solution of **8b** in the air for 1 h, followed by solvent removal and washings with petroleum ether. Yield: essentially quantitative. Calcd for C$_{58}$H$_{49}$NBF$_{24}$O$_2$PRu: C, 50.1; H, 3.55; N, 1.0. Found: C, 50.0; H, 3.52; N, 0.9. ^{1}H NMR (400 MHz, CDCl$_3$, 298 K): δ 0.67 (m, 3 H), 0.98 (m, 3 H), 1.42 (m, 3 H), 1.57 (m, 3H) [P(CH(CH_3)$_2$)$_2$], 1.27 [s, 15 H, C$_5$(CH_3)$_5$], 2.51, 2.57 [m, 1 H each, P(CH(CH$_3$)$_2$)$_2$], 3.40 (dd, $^2J_{HH}$ = 17.4 Hz, $^2J_{HP}$ = 5.1 Hz, 1 H, PCH_aH$_b$), 3.73 (dd, $^2J_{HH}$ = 17.4 Hz, $^2J_{HP}$ = 13.6 Hz, 1 H, PCH$_a$$H_b$), 7.28 (d), 7.38 (m), 7.82 (d), 7.98 (t), 8.16 (d), 8.61 (d) (C$_9H_6$N). ^{31}P{^{1}H} NMR (161.89 MHz, CDCl$_3$, 298 K): δ 75.3 (s). ^{13}C{^{1}H} NMR (101 MHz, CD$_2$Cl$_2$, 298 K): δ 9.36 [s, C$_5$(CH_3)$_5$], 18.09, 18.69, 19.22, 19.68 [s, P(CH(CH_3)$_2$)$_2$], 24.94 [d, $^1J_{CP}$ = 21.1 Hz, PCH(CH$_3$)$_2$], 28.49 [d, $^1J_{CP}$ = 26 Hz, PCH(CH$_3$)$_2$], 39.07 (d, $^1J_{CP}$ = 24.4 Hz, PCH_2), 95.76 [s, C$_5$-(CH$_3$)$_5$], 107.16, 120.78, 128.98, 133.60, 142.77, 148.82, 166.36 (C$_9$H$_6$N).

[Cp*Ru(κ^2-P,N-^{i}Pr$_2$PCH$_2$Py)][BAr′$_4$] (10a). To an equimolar mixture of **1a** and NaBAr′$_4$ (0.5 mmol) under argon was added thoroughly degassed fluorobenzene (20 mL). A blue color developed. The mixture was stirred under argon for 30 min. Then it was filtered through an anhydrous Na$_2$SO$_4$ plug. The solvent was removed in vacuo, leaving a blue microcrystalline solid, which was washed with one portion of petroleum ether and dried in vacuo. The complex turned brown in a few days even when stored under argon at −20 °C. Yield: essentially quantitative. Calcd for C$_{54}$H$_{47}$NBF$_{24}$PRu: C, 49.6; H, 3.62; N, 1.1. Found: C, 49.5; H, 3.52; N, 1.0. ^{1}H NMR (600 MHz, fluorobenzene-d_5, 238 K): δ 0.18 (m, 3 H), 1.00 [m, 7 H, 6 H P(CH(CH_3)$_2$)$_2$ + 1 H PCH_aH$_b$], 1.13 (m, 3 H) [P(CH(CH_3)$_2$)$_2$], 1.63 [s, 15 H, C$_5$(CH_3)$_5$], 2.04, 2.18 [m, 1 H each, P(CH(CH$_3$)$_2$)$_2$], 2.79 (dd, $^2J_{HH}$ = 15.5 Hz, $^2J_{HP}$ = 11.9 Hz, 1 H, PCH$_a$$H_b$), 7.11 (d), 7.26 (m), 7.50 (d), 7.98 (t), 8.57 (d) (C$_5H_4$N). ^{31}P{^{1}H} NMR (242.84 MHz, fluorobenzene-d_5, 238 K): δ 78.3 (s). ^{13}C{^{1}H} NMR (151.5 MHz, fluorobenzene-d_5, 238 K): δ 9.89 [s, C$_5$(CH_3)$_5$], 14.84, 17.13, 17.29, 18.65 [s, P(CH(CH_3)$_2$)$_2$], 21.50 [d, $^1J_{CP}$ = 20.7 Hz, PCH(CH$_3$)$_2$], 25.39 [d, $^1J_{CP}$ = 24.5 Hz, PCH(CH$_3$)$_2$], 30.98 (d, $^1J_{CP}$ = 18.1 Hz, PCH_2), 80.2 [br, C$_5$(CH$_3$)$_5$], 124.10, 130.10, 138.98, 154.6 (C$_5$H$_4$N).

Solution NMR Study of the Protonation Reactions. Solutions of the respective trihydride complexes **2a** and **2b** (0.1 mmol) in CD$_2$Cl$_2$ unless otherwise stated, prepared under an argon

Table 2. Summary of Crystallographic Data for **1b**, **2b**, **3a**, **5b**, **8b**, and **9b**

	1b	**2b**	**3a**	**5b**	**8b**	**9b**
formula	$C_{26}H_{37}ClNPRu$	$C_{26}H_{40}NPRu$	$C_{29}H_{44}NO_3Pru$	$C_{58}H_{51}BF_{24}NPRu$	$C_{58}H_{49}BF_{24}N_3PRu$	$C_{58}H_{49}BF_{24}NO_2PRu$
fw	531.06	498.63	586.69	1360.85	1386.85	1390.83
T (K)	100(2)	100(2)	100(2)	100(2)	100(2)	100(2)
cryst size (mm)	0.60 × 0.34 × 0.06	0.48 × 0.37 × 0.17	0.41 × 0.26 × 0.17	0.40 × 0.37 × 0.18	0.54 × 0.47 × 0.37	0.56 × 0.50 × 0.27
cryst syst	monoclinic	triclinic	monoclinic	monoclinic	monoclinic	monoclinic
space group	$P2_1/n$ (No. 14)	$P\bar{1}$ (No. 2)	$P2_1/n$ (No. 14)	$P2_1/c$ (No. 14)	$P2_1/c$ (No. 14)	$P2_1/c$ (No. 14)
cell parameters						
a (Å)	11.823(2)	8.8380(18)	14.821(3)	20.381(4)	12.711(3)	19.858(4)
b (Å)	16.431(3)	10.743(2)	11.056(2)	12.780(3)	28.273(6)	13.128(3)
c (Å)	12.598(3)	14.114(3)	17.174(3)	23.367(5)	17.368(4)	22.633(5)
α (deg)		93.17(3)				
β (deg)	98.45(3)	92.68(3)	90.64(3)	107.12(3)	110.96(3)	103.11(3)
γ (deg)		112.14(3)				
volume (Å^3)	2420.7(8)	1236.1(5)	2814.0(9)	5817(2)	5829(3)	5747(2)
Z	4	2	4	4	4	4
ρ_{calc} (g cm^{-3})	1.457	1.340	1.385	1.554	1.580	1.607
μ(Mo Kα) (mm^{-1})	0.838	0.711	0.644	0.413	0.415	0.423
F(000)	1104	524	1232	2744	2792	2800
max and min transmn factors	0.932, 0745	0.879, 0.745	0.925, 0.830	0.935, 0.741	0.843, 0.811	0.901, 0.756
θ range for data collection	2.05 < θ < 27.52	2.05 < θ < 27.60	1.80 < θ < 27.59	1.82 < θ < 25.05	1.86 < θ < 27.04	1.05 < θ < 25.12
reflns collected	19 861	10 561	22 894	35 587	46 649	38 322
unique reflns	5518 (R_{int} = 0.0393)	5568 (R_{int} = 0.0172)	6434 (R_{int} = 0.0326)	10 028 (R_{int} = 0.0747)	12 637 (R_{int} = 0.0331)	10 201(R_{int} = 0.0272)
no. of obsd reflns ($I > 2\sigma_I$)	5201	5444	5645	7223	11 434	9461
no. of param	280	280	340	810	815	802
final R1, wR2 values ($I > 2\sigma_I$)	0.0335, 0.0806	0.0247, 0.0610	0.0328, 0.0767	0.0621, 0.1221	0.0381, 0.0940	0.0538, 0.1235
final R1, wR2 values (all data)	0.0365, 0.0828	0.0253, 0.0615	0.0404, 0.0799	0.1005, 0.1348	0.0437, 0.0972	0.0588, 0.1268
residual electron density peaks (e Å^{-3})	+0.815, −0.925	+0.629, −0.796	+0.892, −0.436	+0.753, −0.415	+0.772, −0.658	+2.696, −1.336

atmosphere in NMR tubes, were frozen by immersion into liquid nitrogen. The corresponding amount of proton donor (0.1 mmol of either PhCOOH, indole, or salicylic acid) or CF_3SO_3H (via micropipet: 0.1 mmol for **4a**/**4b**; 0.3 mmol for **6a**/**6b**; 0.2 mmol for **7a**) was added. The solvent was allowed to melt. Then, the tubes were shaken, to mix the reagents, and stored in an ethanol/liquid nitrogen bath. The samples prepared in this way were studied by NMR at low temperatures. The sample was removed from the bath and inserted into the precooled probe of the Varian UNITY-400 spectrometer at 193 K. Once shims were adjusted, the probe was warmed to the desired temperature. The NMR temperature controller was previously calibrated against a MeOH sample, with the reproducibility being ±0.5 °C.

Selected Spectral Data for [Cp*RuH$_3$(κ^1-P-^{i}Pr$_2$PCH$_2$PyH)][CF$_3$SO$_3$] (4a) and [Cp*RuH$_3$(κ^1-P-^{i}Pr$_2$PCH$_2$QuinH)][CF$_3$SO$_3$] (4b). Data for **4a**. ^{1}H NMR (400 MHz, CD_2Cl_2, 203 K): δ −11.36 [br, 3 H, $(T_1)_{min}$ = 213 ms, RuH_3]; 0.76 (m, 6 H), 0.95 (m, 6 H), 1.89 [s, 15 H, C$_5$(CH_3)$_5$], 1.90 [m, 2 H, P(CH(CH$_3$)$_2$)$_2$], 3.07 (d, 2 H, d, $^2J_{HP}$ = 7.8 Hz, PCH_2), 7.75 (t), 7.90 (d), 8.30 (t), 8.54 (d) (C$_5H_4$N), 13.84 (br, 1 H, NH). ^{31}P{^{1}H} NMR (161.89 MHz, CD_2Cl_2, 203 K): δ 98.9 (br).

Data for **4b**. ^{1}H NMR (400 MHz, CD_2Cl_2, 203 K): δ −11.20 [br, 3 H, $(T_1)_{min}$ = 109 ms, RuH_3], 0.81 (m, 6 H), 0.96 (m, 6 H), 1.92 [s, 15 H, C$_5$(CH_3)$_5$], 1.95 [m, 2 H, P(CH(CH$_3$)$_2$)$_2$], 3.26 (d, 2 H, d, $^2J_{HP}$ = 9.2 Hz, PCH_2), 7.70 (t), 7.80 (m), 7.89 (t), 7.99 (d), 8.15 (d), 8.51 (br) (C$_9H_6$N), 13.50 (br, 1 H, NH). ^{31}P{^{1}H} NMR (161.89 MHz, CD_2Cl_2, 203 K): δ 97.9 (br).

Selected Spectral Data for [Cp*RuH$_4$(κ^1-P-^{i}Pr$_2$PCH$_2$PyH)][CF$_3$SO$_3$]$_2$ (6a) and [Cp*RuH$_4$(κ^1-P-^{i}Pr$_2$PCH$_2$QuinH)][CF$_3$SO$_3$]$_2$ (6b). Data for **6a**. ^{1}H NMR (400 MHz, CD_2Cl_2, 203 K): δ −8.09 [br, 4 H, $(T_1)_{min}$ = 13.9 ms, RuH_4], 0.90 (m, 12 H), 1.97 [s, 15 H, C$_5$(CH_3)$_5$], 2.31 [m, 2 H, P(CH(CH$_3$)$_2$)$_2$], 3.56 (d, 2 H, d, $^2J_{HP}$ = 4.6 Hz, PCH_2), 7.75 (d), 7.90 (t), 8.52 (t), 8.67 (br) (C$_5H_4$N), 14.80 (br, 1 H, NH). ^{31}P{^{1}H} NMR (161.89 MHz, CD_2Cl_2, 203 K): δ 79.0 (br).

Data for **6b**. ^{1}H NMR (400 MHz, CD_2Cl_2, 203 K): δ −7.96 [br, 4 H, $(T_1)_{min}$ = 12.4 ms, RuH_4], 0.92 (m, 6 H), 1.02 (m, 6 H), 1.96 [s, 15 H, C$_5$(CH_3)$_5$], 2.37 [m, 2 H, P(CH(CH$_3$)$_2$)$_2$], 3.52 (d, 2 H, d, $^2J_{HP}$ = 8.5 Hz, PCH_2), 7.51 (d), 7.95 (t), 8.15 (t), 8.21 (m), 8.23 (m), 8.93 (d) (C$_9H_6$N), 13.80 (br, 1 H, NH). ^{31}P{^{1}H} NMR (161.89 MHz, CD_2Cl_2, 203 K): δ 80.4 (br).

Selected Spectral Data for [Cp*RuH(CF$_3$SO$_3$)(κ^2-P,N-^{i}Pr$_2$PCH$_2$Py)][CF$_3$SO$_3$] (7a). ^{1}H NMR (400 MHz, CD_2Cl_2, 298 K): δ −5.53 (br, 1 H, RuH); 0.84 (m, 3 H), 1.17 (m, 6 H), 1.49 (m, 3 H), 1.64 [P(CH(CH_3)$_2$)$_2$], 1.80 [s, 15 H, C$_5$(CH_3)$_5$], 2.30, 2.38 [m, 1 H each, P(CH(CH$_3$)$_2$)$_2$], 3.61 (1 H, dd, $^2J_{HH}$ = 17.1 Hz, $^2J_{HP}$ = 7.3 Hz, PCH_aH$_b$), 3.93 (dd, $^2J_{HH}$ = 17.1 Hz, $^2J_{HP}$ = 14.0 Hz, 1 H, PCH$_a$$H_b$), 7.67 (t), 7.85 (d), 8.12 (t), 8.47 (d) (C$_5H_4$N). ^{31}P{^{1}H} NMR (161.89 MHz, CD_2Cl_2, 298 K): δ 92.3 (br). ^{13}C{^{1}H} NMR (101 MHz, CD_2Cl_2, 298 K): δ 10.49 [s, C$_5$(CH_3)$_5$], 17.99, 18.19, 19.12, 20.13 [s, P(CH(CH_3)$_2$)$_2$], 25.99 [d, $^1J_{CP}$ = 24.5 Hz, PCH(CH$_3$)$_2$], 29.15 [d, $^1J_{CP}$ = 26.5 Hz, PCH(CH$_3$)$_2$], 41.10 (br, PCH_2), 103.26 (s, C$_5$(CH$_3$)$_5$), 125.09, 126.35, 142.23, 154.16, 163.16 (C$_5$H$_4$N). ^{19}F NMR (376.28 Hz, CD_2Cl_2, 298 K) δ −78.6 (s).

DFT Calculations. DFT calculations were performed with the *Gaussian 03* package[64] using the hybrid functional M05-2X.[65] The ruthenium atom was described with the Stuttgart pseudopotential SDD[66] for the core electrons and its related basis set for the outer ones, with an added set of f polarization functions with exponent 1.235.[67] Two different basis sets were used for the other atoms: geometry optimizations and thermal corrections (Gibbs energy) were calculated with a 6-31g(d,p) double-ζ basis set including polarization functions in all atoms. Single-point calculations in solvent were performed with the triple-ζ basis set 6-311++G(2d,2p) with two sets of polarization functions and a diffuse function in all atoms.[64]

Solvent calculations were carried out with the CPCM continuum model[68,69] with default parameters for DCM as the solvent (ε = 8.93). If it is not stated otherwise, all of the energies referred to in the text are Gibbs energies in the solvent. These Gibbs energies in the solvent were calculated following the equation $G_{solv} = E_{solv}^{BS2} + (G_{gas}^{BS1} - E_{gas}^{BS1})$.[70]

X-ray Structure Determinations. Single crystals of compounds **1b**, **2b**, **3a**, **5b**, **8b**, and **9b** were obtained and mounted on a glass fiber to carry out the crystallographic study. Crystal data and experimental details are given in Table 2. The X-ray diffraction data collection was measured at 100 K on a Bruker Smart APEX CCD three-circle diffractometer using a sealed tube source with graphite-monochromated Mo Kα radiation (λ = 0.710 73 Å) at the Servicio Central de Ciencia y Tecnología de la Universidad de Cádiz. In each case, four sets of frames were recorded over a hemisphere of the reciprocal space by an ω scan with $\delta(\omega)$ = 0.30° and an exposure of 10 s per frame. Correction for absorption was applied by scans of equivalents using the program *SADABS*.[71] An insignificant crystal decay correction was also applied. The structure was solved by direct methods, completed by subsequent difference Fourier syntheses and refined on F^2 by full-matrix least-squares procedures using the programs contained in the *SHELXTL* package.[72] Non-hydrogen atoms were refined with anisotropic displacement parameters. The program *ORTEP-3*[73] was used for plotting.

Acknowledgment. We thank the Spanish Ministerio de Ciencia e Innovación (DGICYT; Projects CTQ2007 60137/BQU and CTQ2008-06866-C02-01/BQU and Consolider Ingenio-2010 CSD2007-00006) and Junta de Andalucía (Projects PAI FQM188 and P08 FQM 03538) for financial support and Johnson Matthey plc for generous loans of ruthenium trichloride. S.M. acknowledges a FPI fellowship from the Spanish MICINN.

Supporting Information Available: Crystallographic data in CIF format for complexes **1b**, **2b**, **3a**, **5b**, **8b**, and **9b**, tables of

(64) Frisch, M. J.; Trucks, G. W.; Schlegel, H. B.; Scuseria, G. E.; Robb, M. A.; Cheeseman, J. R.; Montgomery, J. A. J.; Vreven, T.; Kudin, K. N.; Burant, J. C.; Millam, J. M.; Iyengar, S. S.; Tomasi, J.; Barone, V.; Mennucci, B.; Cossi, M.; Scalmani, G.; Rega, N.; Petersson, G. A.; Nakatsuji, H.; Hada, M.; Ehara, M.; Toyota, K.; Fukuda, R.; Hasegawa, J.; Ishida, M.; Nakajima, T.; Honda, Y.; Kitao, O.; Nakai, H.; Klene, M.; Li, X.; Knox, J. E.; Hratchian, H. P.; Cross, J. B.; Adamo, C.; Jaramillo, J.; Gomperts, R.; Stratmann, R. E.; Yazyev, O.; Austin, A. J.; Cammi, R.; Pomelli, C.; Ochterski, J. W.; Ayala, P. Y.; Morokuma, K.; Voth, G. A.; Salvador, P.; Dannenberg, J. J.; Zakrzewski, V. G.; Dapprich, S.; Daniels, A. D.; Strain, M. C.; Farkas, O.; Malick, D. K.; Rabuck, A. D.; Raghavachari, K.; Foresman, J. B.; Ortiz, J. V.; Cui, Q.; Baboul, A. G.; Clifford, S.; Cioslowski, J.; Stefanov, B. B.; Liu, G.; Liashenko, A.; Piskorz, P.; Komaromi, I.; Martin, R. L.; Fox, D. J.; Keith, T.; Al-Laham, M. A.; Peng, C. Y.; Nanayakkara, A.; Challacombe, M.; Gill, P. M. W.; Johnson, B.; Chen, W.; Wong, M. W.; Gonzalez, C.; Pople, J. A. *Gaussian 03*, revision C.02; Gaussian, Inc.: Wallingford, CT, **2004**.

(65) Zhao, Y.; Schultz, E.; Truhlar, D. G. *J. Chem. Theory Comput.* **2006**, *2*, 364–382.

(66) Dolg, M.; Stoll, H.; Preuss, H.; Pitzer, R. M. *J. Phys. Chem.* **1993**, *97*, 5852–5859.

(67) Ehlers, A. W.; Böhme, M.; Dapprich, S.; Gobbi, A.; Höllwarth, A.; Jonas, V.; Köhler, K. F.; Stegmen, R.; Veldkamp, A.; Frenking, G. *Chem. Phys. Lett.* **1993**, *1−2*, 111–114.

(68) Barone, V.; Cossi, M. *J. Phys. Chem. A* **1998**, *102*, 1995–2001.

(69) Cossi, M.; Rega, N.; Scalmani, G.; Barone, V. *J. Comput. Chem.* **2003**, *23*, 669–81.

(70) Braga, A. A. C.; Ujaque, G.; Maseras, F. *Organometallics* **2006**, *25*, 3647–3658.

(71) Sheldrick, G. M. *SADABS*; University of Göttingen: Göttingen, Germany, **2001**.

(72) Sheldrick, G. M. *SHELXTL: Crystal Structure Analysis Package*, version 6.10; Bruker AXS: Madison, WI, **2000**.

(73) Farrugia, L. J. *ORTEP-3 for Windows*, version 1.076. *J. Appl. Crystallogr.* **1997**, *30*, 565.

Cartesian coordinates and total energies for all of the optimized structures, and a comparison of computed and X-ray geometrical parameters for **5b**/**5a**. This material is available free of charge via the Internet at http://pubs.acs.org. The crystal structures have also been deposited with the Cambridge Crystallographic Data Centre as CCDC 772200−772205. These coordinates can be obtained, upon request, from the Director, Cambridge Crystallographic Data Centre, 12 Union Road, Cambridge CB2 1EZ, U.K.